The Impaired Wound Healing Process Is a Major Factor in Remodeling of the Corneal Epithelium in Adult and Adolescent Patients With Keratoconus

Katarzyna Jaskiewicz,[1] Magdalena Maleszka-Kurpiel,[2,3] Eliza Matuszewska,[4] Michał Kabza,[5] Malgorzata Rydzanicz,[6] Robert Malinowski,[7] Rafal Ploski,[6] Jan Matysiak,[4] and Marzena Gajecka[1,5]

[1]Institute of Human Genetics, Polish Academy of Sciences, Poznan, Poland
[2]Optegra Eye Health Care Clinic in Poznan, Poznan, Poland
[3]Department of Optometry, Chair of Ophthalmology and Optometry, Poznan University of Medical Sciences, Poznan, Poland
[4]Chair and Department of Inorganic and Analytical Chemistry, Poznan University of Medical Sciences, Poznan, Poland
[5]Chair and Department of Genetics and Pharmaceutical Microbiology, Poznan University of Medical Sciences, Poznan, Poland
[6]Department of Medical Genetics, Medical University of Warsaw, Warsaw, Poland
[7]Institute of Plant Genetics, Polish Academy of Sciences, Poznan, Poland

Correspondence: Marzena Gajecka, Institute of Human Genetics, Polish Academy of Sciences, Strzeszynska 32, Poznan 60-479, Poland; gamar@man.poznan.pl.

KJ and MMK contributed equally to this work.

Received: September 16, 2022
Accepted: January 27, 2023
Published: February 22, 2023

Citation: Jaskiewicz K, Maleszka-Kurpiel M, Matuszewska E, et al. The impaired wound healing process is a major factor in remodeling of the corneal epithelium in adult and adolescent patients with keratoconus. *Invest Ophthalmol Vis Sci.* 2023;64(2):22. https://doi.org/10.1167/iovs.64.2.22

Purpose. Keratoconus (KTCN) is the most common corneal ectasia, characterized by pathological cone formation. Here, to provide an insight into the remodeling of the corneal epithelium (CE) during the course of the disease, we evaluated *topographic* regions of the CE of adult and adolescent patients with KTCN.

Methods. The CE samples from 17 adult and 6 adolescent patients with KTCN, and 5 control CE samples were obtained during the CXL and PRK procedures, respectively. Three *topographic* regions, *central*, *middle*, and *peripheral*, were separated toward RNA sequencing and MALDI-TOF/TOF Tandem Mass Spectrometry. Data from transcriptomic and proteomic investigations were consolidated with the morphological and clinical findings.

Results. The critical elements of the wound healing process, epithelial–mesenchymal transition, cell–cell communications, and cell–extracellular matrix interactions were altered in the particular corneal *topographic* regions. Abnormalities in pathways of neutrophils degranulation, extracellular matrix processing, apical junctions, IL, and IFN signaling were revealed to cooperatively disorganize the epithelial healing. Deregulation of the epithelial healing, G2M checkpoints, apoptosis, and DNA repair pathways in the *middle* CE *topographic* region in KTCN explains the presence of morphological changes in the corresponding *doughnut* pattern (a thin cone center surrounded by a thickened annulus). Despite similar morphological characteristics of CE samples in adolescents and adults with KTCN, their transcriptomic features were different. Values of the posterior corneal elevation differentiated adults with KTCN from adolescents with KTCN and correlated with the expression of *TCHP*, *SPATA13*, *CNOT3*, *WNK1*, *TGFB2*, and *KRT12* genes.

Conclusions. Identified molecular, morphological, and clinical features indicate the effect of impaired wound healing on corneal remodeling in KTCN CE.

Keywords: cornea, corneal epithelium, corneal wound healing, keratoconus, MALDI-TOF/TOF Tandem Mass Spectrometry, posterior corneal elevation, proteomics, transcriptomics

Keratoconus (KTCN) is the most common corneal ectasia, characterized by the conical shape of the cornea, leading to substantial vision impairment. KTCN is described as bilateral, but often manifests as a highly asymmetric disorder.[1] The disease usually occurs in adolescence and progresses through the third or fourth decades of life.[2]

KTCN affects the general population with the prevalence assessed at 1.38 per 1000 individuals, but strongly differs regarding gender and ethnicity.[3] There are no current data available concerning the KTCN prevalence in Poland. The hospital-based epidemiological study had not revealed KTCN frequency, however, showed that 64% of patients with KTCN were male.[4] According to the Polish Health Problem Card, the estimated prevalence of KTCN is 200 to 250 per 100,000 residents.[5]

KTCN is a multifactorial disease with a nebulous etiology. Environmental components including UV exposure and lifestyle habits (eye rubbing, contact lens wear) have been

thoroughly indicated.[6,7] Also, a complex genetic background comprising numerous identified KTCN loci, candidate genes, and pathways have been revealed.[8–11]

In KTCN diagnosis, various diagnostic methods based on the mapping of both epithelium and corneal thickness, as well as the anterior and posterior corneal surface topography assisted with advanced computer software, are being used.[12] Changes in the posterior surface of the cornea are often the earliest observed feature of KTCN.[13] In contrast, the topographically "normal" eye of a patient with KTCN may have features of KTCN detectable by the epithelial thickness mapping.[1] The automated computerized algorithm's data allow pointing to a clear distinction between unaffected and KTCN corneas based solely on epithelial and stromal thickness parameters.

KTCN is the second leading cause of corneal transplantation worldwide,[14] although the traditional penetrating keratoplasty performed in the advanced disease state is being frequently replaced by deep lamellar keratoplasty.[11] The management of mild to moderate KTCN is primarily aimed at improving visual acuity with glasses, contact lenses (rigid gas permeable), and intracorneal ring segments implantation, or a combination of these modalities.[15] In addition, the corneal collagen cross-linking (CXL) has been implemented successfully as a treatment option to stiffen the cornea and halt the progression of KTCN.[16–18]

Histopathological abnormalities in KTCN corneas comprise all corneal layers, of which the most characteristic or symptomatic are epithelial thinning, breaks in Bowman's layer,[19] the presence of apoptotic cells in physiologically acellular Bowman's membrane, and Descemet's membrane disruptions.[20] Irregular cell arrangement and cell loss in the corneal epithelium (CE) and stroma were also observed.[21]

The KTCN cone, observed as a presumable consequence of multilevel structural and functional changes in corneal tissue, including those in the epithelium (superficial, wing, basal),[22–25] speaks for a study design based on separately assessed, differently affected *topographic* regions of the CE. In this study, taking into account corneal thickness, especially the epithelial thickness, including the thinnest epithelium on the top of the KTCN cone, and the location of the apex or center of the cone in the cornea, three *topographic regions* of the CE, *central*, *middle*, and *peripheral*, were chosen to be investigated separately in patients with KTCN, and then compared with the adequate material derived from control individuals.

We hypothesize that molecular abnormalities in the CE of patients with KTCN are divergent in particular *topographic* regions, and, therefore, they shape the *doughnut* pattern in the morphologically disturbed CE in KTCN. Moreover, these molecular and morphological changes in particular regions of the CE may reflect an interplay between stroma and epithelium. Because corneal curvature abnormalities worsen as the disease progresses and to provide insight into the role of CE remodeling in KTCN, we examined numerous features comparing adolescent and adult patients. We undertook histological and transcriptomic profiling of the CE and proteomic assessments, pointing to discriminative clinical and molecular features in the assessed *topographic* regions of the CE in patients with KTCN.

Here we present the comprehensive evaluation of clinical, morphological, transcriptomic, and proteomic data concerning the three *topographic* regions of the CE in adult and adolescent patients with KTCN, evaluated together and separately in the studied subgroups.

Methods

Ophthalmic Examination and Patients' Inclusion and Exclusion Criteria

We included three subgroups of patients: adults with KTCN, adolescents with KTCN, and control individuals (the non-KTCN mild myopia patients). Each individual underwent a complete ophthalmological examination, including the assessments of both uncorrected and best corrected visual acuity, IOP, corneal tomography with rotating Scheimpflug camera WaveLight Oculyzer II (Alcon, Fort Worth, TX, USA), epithelial thickness mapping spectral-domain optical coherence tomography device (Zeiss Cirrus 5000, Carl Zeiss Meditec, Dublin, CA, USA), slit-lamp, and dilated funduscopic examination. The inclusion and exclusion criteria for adults and adolescents with KTCN, and control individuals are described in details in Supplementary Material 1.1.

A questionnaire comprising the behavioral, environmental, and socioeconomic aspects, including eye rubbing, use of contact lenses, atopy, UV exposure, smoking, reading habits, time spent in front of a screen (computer, tablet, smartphone, or electronic reader), hormone intake, education level, and place of living, was completed by each participant. JASP Software[26] was used in statistical analyses of clinical parameters, and the tests applied are described in Supplementary Material 1.2.

CXL and Photorefractive Keratectomy (PRK) Procedures

CXL in patients with KTCN was performed in accordance with the standard Dresden protocol,[27–29] and PRK was performed as a refractive error correction procedure[30] in control individuals, as described in Supplementary Material 1.3 and 1.4.

Material Collection and Sample Preparation

Stamps toward the nose and eyebrow were made on the CE before the excision in the CXL and PRK procedures to enable correct tissue orientation during cutting and separation of the *topographic* regions. The obtained tissues were submersed in an RNA stabilization solution (RNAlater; Qiagen, Hilden, Germany) immediately after excision and stored at −80°C until nucleic acids and proteins isolation. Further details of the sample preparation are included in Supplementary Material 1.5.

The procedure of designation of the particular *topographic* region is shown in Figures 1D, E, and Supplementary Figure S1. Before the CE cutting, the epithelium thickness values measured automatically using the OCT for the particular regions of CE were evaluated. Then, the specific *topographic* regions were assessed manually together with the determination of cone and apex (for KTCN and controls, respectively) location (central, superior or inferior, and nasal or temporal) at the same time by the operating surgeon and the researcher processing the material.

Assessment of Morphological Abnormalities in CE

Nuclei cell morphology and density in *topographic* regions of the assessed epithelia, in both patients with KTCN and

Investigative Ophthalmology & Visual Science

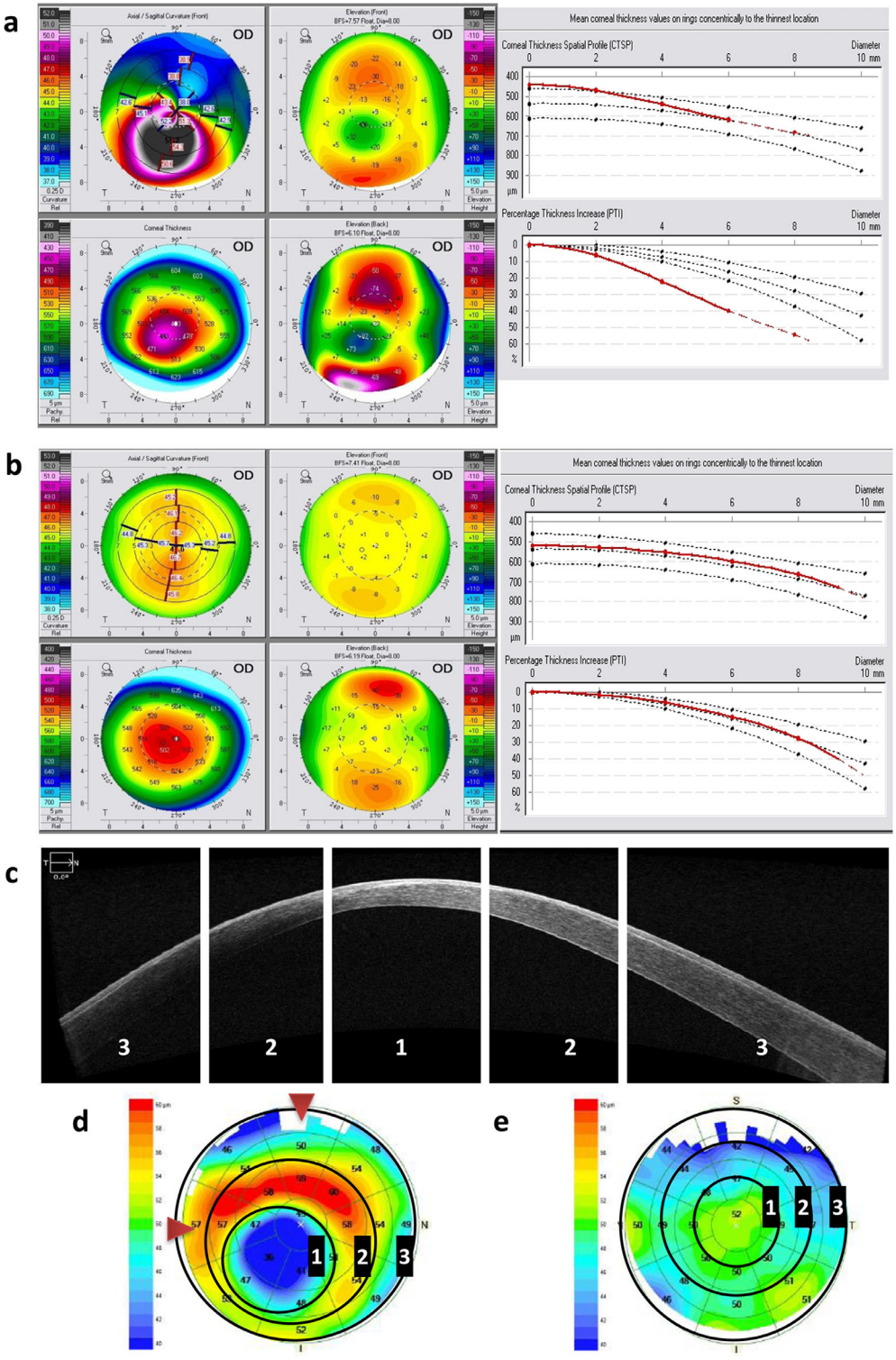

Figure 1. Results of ophthalmological examination of KTCN and control individuals, and the designation of corneal *topographic* regions. Differences between KTCN and control cornea in axial curvature, corneal thickness, anterior elevation, and posterior elevation levels are presented, based on the corneal tomography results obtained with rotating Scheimpflug camera WaveLight Oculyzer II for (**A**) the KTCN adult patient (4 OPT/KTCN/OD) and (**B**) control individual (1 OPT/M/OS). For the exact values of parameters evaluated, check the Supplementary Table S2. In the control cornea, the steepest part of the organ, called the apex, is most often located centrally on the visual axis, in the case of KTCN, the corneal apex is decentered off. (**C**) The cross-sectional image of the cornea and the segment of the anterior eye (spectral-domain optical coherence tomography [SD-OCT]) with indicated three distinct *topographic* regions (1, *central*; 2, *middle*; 3, *peripheral*) in KTCN patient 17 OPT/KTCN/OS. The decreased epithelial thickness and stromal thinning at the *central* region are shown. (**D, E**). The *topographic* regions—1, *central*; 2, *middle*; and 3, *peripheral*—are designated based on the steepness of epithelial thickness in KTCN (**D**, 4 OPT/KTCN), and control individual (**E**, 1 OPT/M), respectively. (**D**) The red arrows indicate the stamps for the correct tissue orientation, made before the CE removal during the CXL procedure. Then, the designated CE *topographic* regions were separated and processed further.

controls, were evaluated as described in Supplementary Material 1.6. At least 100 nuclei and the surface of 12,000 µm^2 of each *topographic* region were screened.

RNA and Protein Extraction

Separated CE samples were transferred from the microscope slides to the lysis solution (Norgen Biotek, Thorold, Ontario, Canada). Total RNA, DNA, and proteins were extracted and purified according to the instructions supplied with the RNA/DNA/Protein Purification Plus Micro Kit (Norgen Biotek). RNA extraction included DNase I treatment (RNase-Free DNase Set, Qiagen). The quality and quantity of the purified RNA and protein samples were assessed as described in Supplementary Material 1.7.

Total RNA Library Preparation and Sequencing and RNA Sequencing (RNA-Seq) Data Analyses

Total RNA libraries were prepared according to a previously established protocol,[31] using TruSeq Stranded Total RNA Library Prep Gold (Illumina, San Diego, CA, USA) in accordance with the manufacturer's protocol and details presented in Supplementary Material 1.8. A 100-bp paired-end sequencing run was performed on a NovaSeq 6000 platform (Illumina). The CE samples were sequenced with an average coverage of 100 million read pairs per sample. Bioinformatic analyses were executed according to a previously established protocol[32] with some modifications as presented in Supplementary Material 1.8.

Genes were considered to be differentially expressed based on the following cutoffs 0.01 false discovery rate threshold value and 1.5-fold change (FC). Reactome[33] pathway enrichment analysis was performed using the CAMERA method implemented in the limma package.[34] Pathways were considered to be differentially expressed based on the cutoff of the 0.01 false discovery rate. The enrichment analysis of hallmarks was executed using a published Hallmark Gene Set Collection being a part of the Molecular Signatures Database. In this approach, each hallmark consists of defined and concise sets of genes to most adequately summarize a specific biological state or process that, by decreasing variation and redundancy, helps in uncovering the most important but hidden molecular signatures.[35]

Bioinformatic analyses, including differential expression analyses and/or hallmarks enrichment, were executed in the following scheme: (1) *central* versus *middle* versus *peripheral* CE regions in each KTCN patient and control individual; (2) *central*, *middle*, or *peripheral* CE region in adult KTCN versus the *central*, *middle*, or *peripheral* region in control individuals; (3) the *central*, *middle*, or *peripheral* CE region in adolescent KTCN versus the *central*, *middle*, or *peripheral* region in control individual; and (4) the *central*, *middle*, or *peripheral* CE region in adolescent KTCN versus the *central*, *middle*, or *peripheral* region in adult KTCN.

RNA-Seq Data Verification Using RT-Quantitative PCR (RT-qPCR)

To verify the RNA-Seq data, the RNA samples used in the original RNA-Seq assessment were reverse transcribed to cDNA with the Maxima First Strand cDNA Synthesis Kit for RT-qPCR, with dsDNase (Thermo Fisher Scientific, Vilnius, Lithuania), according to the manufacturer's procedure. Expression levels of six candidate KTCN genes—*KRT12*, *IFI27*, *TGFB2*, *B4GALT1*, *SPATA13*, *and WNK1*—and two housekeeping transcripts—*B2M* and *GAPDH*—were assessed using the FastStart Essential DNA Green Master (Roche Diagnostics, Penzberg, Germany) according to the manufacturer's protocol, using the CFX96 Touch Real-Time PCR Detection System (Bio-Rad Laboratories, Hercules, CA, USA) in a total volume of 20 µL with 0.5 ng cDNA. Each reaction was performed in duplicate. The primer sequences and annealing temperatures are shown in Supplementary Table S1.

The relative quantification of gene expression was normalized to the level of the GAPDH and B2M transcripts with the comparative CT method. The log2 transformed FC values of gene expression levels between KTCN and control samples were calculated for the RT-qPCR and RNA-Seq data. Pearson correlations between log2 FC values for the evaluated genes were calculated using the JASP Software.[26]

Matrix-Assisted Laser Desorption Ionization Time of Flight (MALDI-TOF/TOF) Tandem Mass Spectrometry Protein–Peptide Profiling, Classification, and Identification of Discriminative Peaks

The methodology is described in detail in Supplementary Material 1.9. MALDI-TOF/TOF Tandem Mass Spectrometry proteomic analysis was performed after tryptic digestion, concentration, and purification of the samples. The research was conducted with an UltrafleXtreme (Bruker Daltonics, Billerca, MA, USA) mass spectrometer in the m/z (mass-to-charge ratio) range of 700 to 3500. The proteomic identification was based on the SwissProt protein sequence database.

Statistical analyses were performed in ClinProTools 3.0 (Bruker Daltonics) software with mathematical classification algorithms. Discriminative peaks for CE samples of adolescents with KTCN (compared with controls) were calculated in JASP Software[26] using statistical tests.

Pathways and Genes of Biological Importance

Consolidation of the obtained transcriptomic, proteomic, and clinical data was performed. Relationships between differentially expressed genes, gene pathways, and enriched hallmarks, and proteomic profile of KTCN specific *topographic* regions of the CE were identified using Venn diagrams and Pearson correlation tests, with an indication of association networks (STRING tool,[36] REACTOME database,[37] and gene ontology enrichment analysis[38]). To complement the results of these analyses, and indicate genes in differentially expressed pathways recognized using the CAMERA method and Hallmark Gene Set Collection, we checked the expression of genes with a mean expression level of at least 1 transcript per million from particular pathway gene sets, comparing the data between the subgroups of samples (the analysis was limited to males due to gender bias), and defined as significant based on the following cutoffs: P value ≤ 0.05 (t-test) and FC ≥ 1.5 or FC ≤ 0.5. The STRING tool,[36] Pathway Commons database,[39] SignaLink 3.0 database,[40] and SIGNOR tool[41] were used for the reconstruction of selected pathways' networks.

The clinical data, including flat keratometric readings (K1), steep keratometric readings (K2), maximum simulated keratometry, anterior elevation, posterior elevation,

Investigative Ophthalmology & Visual Science

difference in best fit sphere, thinnest corneal thickness, axial length, IOP, difference in best fit sphere, and thickness of the *central*, *middle*, and *peripheral* CE region values, were examined in detail using Pearson correlation tests, if correlated with transcriptomic data. Comparative analyses with the data obtained during the assessment of whole thickness corneas[31,32,42,43] are described in Supplementary Material 1.10.

At the same time, the genetic assessment of studied CE samples was performed. The CE samples from four unrelated adolescent patients with KTCN and two control individuals were analysed using the whole genome sequencing. The DNA samples were extracted according to the instructions of the RNA/DNA/Protein Purification Plus Micro Kit (Norgen Biotek), and their quantity was measured by Qubit dsDNA HS Assay Kit (Invitrogen, Thermo Fisher Scientific) and quality was assessed by 1% gel electrophoresis. Whole genome sequencing was performed with a TruSeq Nano DNA HT Library Prep Kit (Illumina) and the HiSeqX platform (Illumina) with mean coverage depth 30× at CloudHealth Genomics (Shanghai, China). The short reads were trimmed using the BBDuk2 program from the BBTools suite (http://jgi.doe.gov/data-and-tools/bbtools/) to remove Illumina adapters and poor-quality regions (mean Phred quality, <5). Then, reads were mapped to reference genome GRCh38 (source: Ensembl release 100) using BWA-MEM.[44] Duplicated reads were marked using Sam Bamba.[45] Single nucleotide polymorphisms and indel calling has been performed using Platypus[46] and the detected variants were annotated using Ensembl Variant Effect Predictor software.[47] The coding and noncoding sequence variation was assessed to show the link with here reported transcriptomic outcomes for the same CE samples.

Data Accessibility

Additional research data are presented in Supplementary Materials. Processed data of the RNA-Seq are shared in Mendeley Data Repository (https://data.mendeley.com/datasets/stpz7s5s5j/draft?a=94dfc03c-4459-40b6-888f-6d40b9a89249, DOI:10.17632/stpz7s5s5j.1). The other data supporting the findings of this study are available from the corresponding author upon reasonable request.

Results

Clinical Characteristics of Patients

There were 17 adult patients with KTCN (2 females and 15 males), 6 adolescent patients with KTCN (2 females and 4 males), and 5 control individuals with mild myopia (2 females and 3 males) involved in this study. The clinical characteristics of the examined individuals and eyes subjected to the surgery are presented in Table 1, and details are compiled in Supplementary Table S2A; Supplementary Table S2B encompasses the information collected for both eyes in the studied individuals. Examples of results of corneal tomography with a rotating Scheimpflug camera and corneal thickness mapping of the examined individuals are presented in Figures 1A, B.

Different values of clinical parameters such as K1, K2, maximum simulated keratometry, anterior elevation, posterior elevation, difference in best fit sphere, TCT, and thickness of *central*, *middle*, and *peripheral* CE regions were found in the subgroups of adults and adolescents with KTCN in comparison with control individuals. The difference between the posterior elevation in adults (58.24 ± 13.89) and adolescents (35.00 ± 13.11) was found (P = 0.0018) (Supplementary Fig. S2). Differences in average values (with standard deviations) comparing the thickness of *central*, *middle*, and *peripheral* CE regions were found (Fig. 2). Other findings concerning both automatically and manually assessed CE thickness values are shown in Supplementary Table S3 and commented on in Supplementary Material 2.1.

The cone and apex locations in the eyes subjected to surgery for KTCN and controls, respectively, are reported in

Table 1. Clinical Characteristics of Examined Individuals and the Eyes Subjected to the Surgery

	Adults with KTCN		Adolescents with KTCN		Controls	
	Average ± SD	**Median**	**Average ± SD**	**Median**	**Average ± SD**	**Median**
Age at examination	27.94 ± 7.96	**25.0**[*]	15.33 ± 1.97	**15.0**[*]	28.00 ± 4.30	30.0
Age at diagnosis KTCN	24.56 ± 7.92	22.5	14.83 ± 2.14	15.0	*n/a*	*n/a*
K1, D	45.77 ± 3.71	45.8[*]	44.8 ± 2.46	44.2[*]	42.72 ± 2.29	43.3
K2, D	45.59 ± 11.11	47.2[*]	47.72 ± 4.00	46.3[*]	43.84 ± 2.11	44.2
K_{max}, D	57.14 ± 5.79	56.8[*]	54.15 ± 7.28	51.95[*]	44.14 ± 2.25	44.4
Anterior elevation, µm	26.88 ± 7.03	24.0[*]	19.67 ± 12.19	13.0[*]	1.60 ± 1.14	2.0
Posterior elevation, µm	**58.24 ± 13.89**	55.0[*,†,‡]	**35.00 ± 13.11**	30.5[*,†,‡]	**1.00 ± 2.74**	1.0
Diff BFS, µm	43.12 ± 19.35	41.0[*]	26.00 ± 20.47	20.5[*]	1.40 ± 1.52	1.0
TCT, µm	459.35 ± 40.06	461.0[*]	440.33 ± 34.99	443.5[*]	517.2 ± 24.12	515.0
AL, mm	24.59 ± 1.13	24.53	23.45 ± 0.82	23.64	24.23 ± 1.10	24.19
IOP, mm Hg	10.75 ± 1.61	11.0	12.80 ± 3.27	13.0	13.75 ± 2.22	14.0
Thinnest epithelial thickness (in range 0.0–7.0 mm), µm	39.65 ± 4.52	39.0[*]	38,50 ± 3.10	39.5[*]	44.00 ± 1.79	45.0
Average thickness of *central* region, µm	40.76 ± 4.13	40.0[*]	40.33 ± 3.08	41.0[*]	50.00 ± 2.35	49.0
Average thickness of *middle* region, µm	53.24 ± 3.11	52.0[*]	51.50 ± 4.09	50.0[*]	47.2 ± 1.92	47.0
Average thickness of *peripheral* region, µm	46.12 ± 1.69	46.0	45.33 ± 1.37	45.0	44.8 ± 3.19	45.0

K1, flat keratometric readings; K2, steep keratometric readings; K_{max}, maximum simulated keratometry; diffBFS, difference in best fit sphere; TCT, thinnest corneal thickness; AL, axial length; n/a, not applicable.

[*] Statistically significant differences between patients with KTCN and controls ($P \leq 0.05$).

[†] Statistically significant differences between patients adults/adolescents subgroups ($P \leq 0.05$).

[‡] $P = 0.0018$.

Investigative Ophthalmology & Visual Science

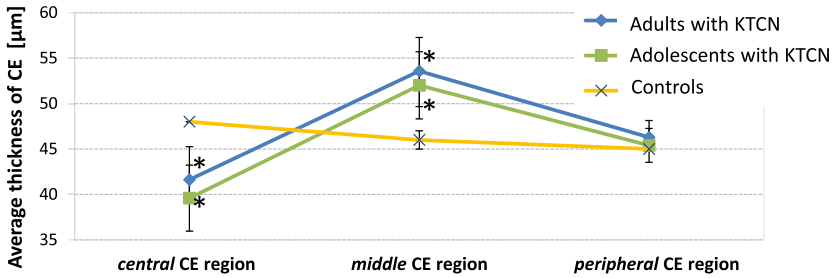

Figure 2. Differences in thickness of *central/middle/peripheral topographic* regions of CE in patients with KTCN and controls, and between patients with KTCN and controls. The average values with standard deviation are presented. *Statistically significant differences between patients' subgroups; for *central* CE region: adults with KTCN versus controls, $P = 0.001$, and adolescents with KTCN versus controls, $P = 0.004$; for *middle* CE region: adults with KTCN versus controls, $P = 0.0008$, and adolescents with KTCN versus controls, $P = 0.0336$.

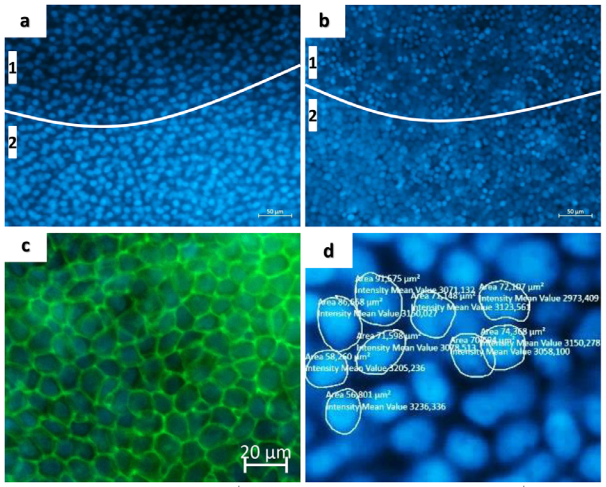

e

	KTCN			CONTROLS		
	Central CE region- 1	*Middle CE region- 2*	*Peripheral CE region- 3*	*Central CE region- 1*	*Middle CE region- 2*	*Peripheral CE region- 3*
nuclei density (nuclei/mm²)	5 250	**7 417**	6 250	5 750	**5 750**	5 417
nucleus surface (µm²)	101	**88**	96	95	**106**	117

Figure 3. The morphology and density of the remodeled CE in KTCN in regions 1 (*central*) and 2 (*middle*) in KTCN (**A**) and control individuals (**B**); staining with DAPI (**A, B, D**) and wheat germ agglutinin (WGA) conjugate (**C**) (Zeiss Imager Z2 with ApoTome.2). (**E**) Average nuclei density and single nucleus surface in the *central*, *middle*, and *peripheral topographic* regions of CE, calculated for two KTCN and two control individuals, based on the microscopic assessment of DAPI stained samples with a screening of 12,000 µm² of each region' surface, and counting of at least 100 nuclei per each CE region. Significant differences are bolded.

Supplementary Table S2A. Both, the central–temporal and inferior–temporal locations were found to be more common in patients with KTCN compared with controls ($P = 0.0048$). According to the project assumption, the analyzed subgroup of adolescent patients with KTCN was definitely different in age at examination (15.33 ± 1.97) compared with adults with KTCN (27.94 ± 7.96) and controls (28.00 ± 4.30). A total of 84 samples of CE (3 *topographic* regions × 28 ascertained individuals) were collected and proceeded in accordance with a study scheme (Supplementary Fig. S1).

The Morphologically Different *Middle* Region of KTCN CE

No morphological differences were found comparing the three assessed *topographic* regions of the CE in controls. The differences in average nuclei density and average single nucleus surface of the *middle* CE region comparing the patients with KTCN and control individuals were revealed (Fig. 3). In line with observations of irregularities visible at epithelial thickness maps, more nuclei (7417/mm² vs. 5750/mm²) and nuclei smaller in size (88 µm² vs. 106 µm²) in the *middle* CE region in patients with KTCN, were observed. We have not noticed morphological differences in the CE samples comparing the adult and adolescent patients with KTCN.

The Impact of Gender in Transcriptomic Profiling

We found that the gender of the studied patients influenced the sample clustering into male and female subgroups in the transcriptomic evaluation, as documented in Supplementary Figure S3A. Consequently, because the majority of our processed samples were derived from male individuals, further bioinformatics analyses were narrowed down to these samples. A UMAP plot after removing the data derived from samples of female patients is presented in Supplementary Figure S3B.

KTCN-Specific Gene Expression Manifested in the *Peripheral* CE Region of Adult Patients With KTCN

In control samples, no differentially expressed genes were identified in the opposing *central*, *middle*, and *peripheral topographic* CE regions. However, comparing the particular *topographic* CE regions of patients with KTCN with the corresponding CE regions of controls, the differentially expressed genes were found, with the majority of them observable in the *peripheral topographic* CE region of adults with KTCN (compared with the *peripheral* CE region in controls) (Supplementary Table S4), in which 258 genes were downregulated (130 protein coding), including *ADAMTS4*, *MEGF11*, *PROX1*, *RAX*, *ANK2*, *NLRP4*, *TRABD2B*, *MUC13*, *VSX1*, *LTF*, *ROS1*, and three upregulated, (*RN7SL2*, *STON2*, and *RN7SL4P*). Moreover, the genes *CDH13*, *EDNRB*, *PTN*, *NUPR1*, *BCL11B*, *SGPP*, *CDH2*, *DCN*, *PTN*, *TRIL*, *RTN4RL1*, and *LRRC3B* showed decreased expression in the *central topographic* region in adults with KTCN compared with the *peripheral* region of CE in these individuals. In contrast, *CYFIP2*, *LEFTY1*, *CLMP*, *DSCAM*, *RGL3*, and *CHST2* were upregulated in the *central* region of the CE.

In adults with KTCN, we found 62 genes with downregulated expression (25 protein coding) in the *peripheral* region of CE, including *KRTAP4-16*, *TBX5*, *ASB5*, *MT-TM*, *MT-TQ*, compared with adolescents with KTCN. No differentially expressed genes for KTCN CE *middle* region were recognized compared with *central* or *peripheral* CE regions in adults and adolescents with KTCN, and comparing the data with the corresponding CE *middle* region of the controls.

Over-represented Immune System Pathways and Under-represented Extracellular Matrix Organization Pathways in CE in Patients With KTCN

Of 984 the KTCN *topographic*-specific pathways, the 10 most differentiated in the comparison of particular CE regions between and within evaluated subgroups are presented in Supplementary Table S5A-O. The IFN alpha-beta signaling, IFN gamma signaling, and overall IFN signaling pathways were enriched within upregulated genes in the *central*, *middle*, and *peripheral topographic* regions of the CE of adults with KTCNcompared with adequate CE regions of controls, whereas, senescence pathways (cellular senescence and senescence-associated secretory phenotype) were mostly enriched in the *peripheral* CE region of adults with KTCN (Supplementary Table S5C). Moreover, the analysis revealed that the upregulated genes were associated with DNA methylation pathway in the *central* CE region of the adults with KTCN and adolescents with KTCN in comparison with controls (Supplementary Table S5D). The same trend of change was observable for the activated PKN1 stimulates transcription of androgen receptor regulated genes KLK2 and KLK3 pathway (Supplementary Table S5A, D). In adolescent patients with KTCN the *middle* CE region disclosed features of the selenoamino acid metabolism and translation-related pathways in analysis within genes with downregulated expression (Supplementary Table S5E).

We also compared the enriched pathways by juxtaposing the particular *topographic* regions with each other in the analysed subgroups of patients (excluding results from the control subgroup, since they may reflect physiologically various gene expressions, Supplementary Tables S5J–O), as described in greater detail in Supplementary Materials 2.3. The results of comparative analyses of CE data with data corresponding with the whole thickness corneas are described in Supplementary Materials 2.3.

Distinct Hallmarks of the *Middle* CE Region of Adult Patients With KTCN

In the hallmark gene set analysis, the apoptosis and G2M checkpoint gene sets were found to be upregulated in *central* and *peripheral* CE, and unchanged in the *middle* region in adults with KTCN, in comparison with the adequate *topographic* region in the CE samples derived from controls. The same trend was revealed for androgen response, DNA repair, MYC targets, peroxisome, protein secretion, unfolded protein response, oxidative phosphorylation, reactive oxygen species pathway, and Wnt beta-catenin signaling hallmarks. These findings do not apply to CE samples derived from adolescents with KTCN. The hallmarks of the IFN alpha response and IFN gamma response were upregulated in all the *topographic* regions of CE patients with KTCN, compared with controls (Table 2, Supplementary Table S6).

RNA-Seq Data Verification Using RT-qPCR

A high positive correlation between the RNA-Seq and RT-qPCR data was found, as presented in Supplementary Table S7. Shown is RT-qPCR data of *GAPDH*, *B2M*, *KRT12*, *IFI27*, *TGFB2*, *B4GALT1*, *SPATA13*, and *WNK1* gene expressions in each of the 84 originally collected CE samples used for FC calculations. Further results are presented in Supplementary Table S8 (log2FC values) and Supplementary Figure S4 ($R^2 = 0.7854$; Pearson correlation coefficient = 0.8857).

Discriminative Proteomic Features in the CE of Adult Patients With KTCN

The total average proteomic spectra of the CE samples of the adults with KTCN and controls are presented in Supplementary Figure S5. Because the two applied chemometric algorithms quick classifier and genetic algorithm are based on different mechanisms, the peaks classified as discriminative between these algorithms are divergent. We identified 11 unique proteins classified as discriminative between the *central* CE region of adults with KTCN versus controls. In a comparison of the *middle* CE region of adults with KTCN versus controls, we identified five proteins differentially expressed, and between *peripheral* CE region of adults with KTCN compared with controls, we identified 14 discriminative proteins. Lists of discriminative m/z ions for each algorithm together with values of chemometric parameters calculated for the algorithms are presented in Supplementary Table S9. A list of identified proteins classified as discriminative between particular CE regions of adults with KTCN and controls, together with the direction of change is presented in Table 3. The chemometric parameters (parameters of cross-validation and recognition capability) calculated for implemented algorithms in particular statistic schemes (e.g., the *central* region of the CE samples of the adults with KTCN vs. controls), assessing the accuracy of the obtained models are indicated in Table 3.

Table 2. Selected Hallmark Pathways Differentially Represented in Particular Regions of CE in Adults and Adolescents With KTCN, in Comparison With Corresponding CE Regions of Controls

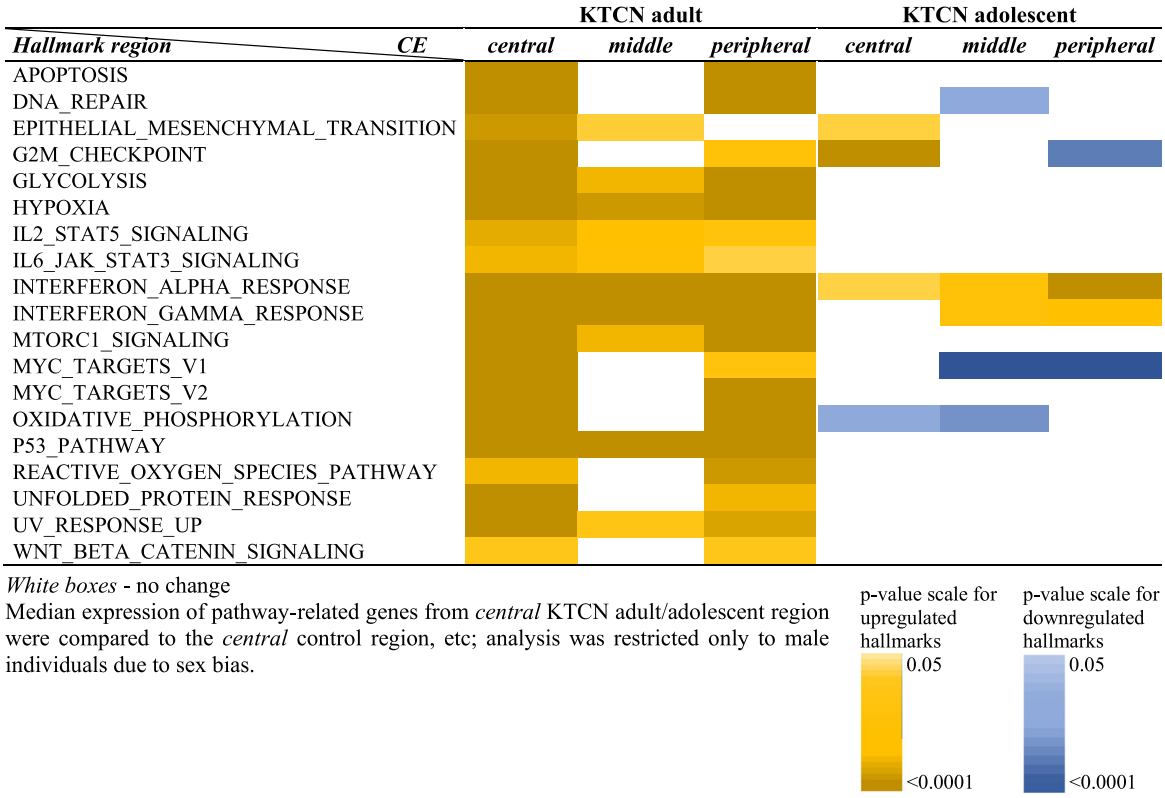

White boxes - no change
Median expression of pathway-related genes from *central* KTCN adult/adolescent region were compared to the *central* control region, etc; analysis was restricted only to male individuals due to sex bias.

Table 3. Identified Proteins Classified as the Discriminative for Adults With KTCN Using Chemometric Algorithms

	***Central* CE Region**		***Middle* CE Region**		***Peripheral* CE Region**	
Direction algorithm	↑	↓	↑	↓	↑	↓
Genetic algorithm	ENO1 PGBD2	HEATR4 CSDE1 TTBK1 SDHA SELENOO TCF20	IGHV3-30	ZBTB4 HSPB1	TKT	IQCF2 WNK4 CLU CHERP
Quick classifier	KRT12 SLC8A1 F199X	HEATR4 SDHA	NDOR1	LENG9	SCN5A PTPRU TBC1D4 IL1RAP F5	RMI1 ABCA13 CLU ANKRD36C

Parameter	Cross-validation (%)	Recognition capability (%)	Cross-validation (%)	Recognition capability (%)	Cross-validation (%)	Recognition capability (%)
Genetic algorithm	95.8	100.0	78.2	100.0	86.5	95.8
Quick classifier	86.8	97.1	67.4	70.3	75.0	91.7

Arrows show the direction of change comparing the specific CE region of adults with KTCN to the corresponding CE region of controls. Values of chemometric parameters calculated for algorithms are indicated.

Molecular Indicators of Specific Clinical Features of KTCN

Based on the correlations of the transcriptomic findings with the clinical data we found the expression of *TCHP* (R = −0.47; $P = 0.029$), *SPATA13* (R = −0.75; P= 6.6e-05), *CNOT3* (R = −0.25; $P = 0.26$), *WNK1* (R = −0.34; $P = 0.12$), *TGFB2* (R = −0.59; $P = 0.0035$), and *KRT12* (R = −0.43; $P = 0.046$) genes to be correlated with the posterior elevation (Fig. 4A). In addition, considering exclusively clinical data of adults

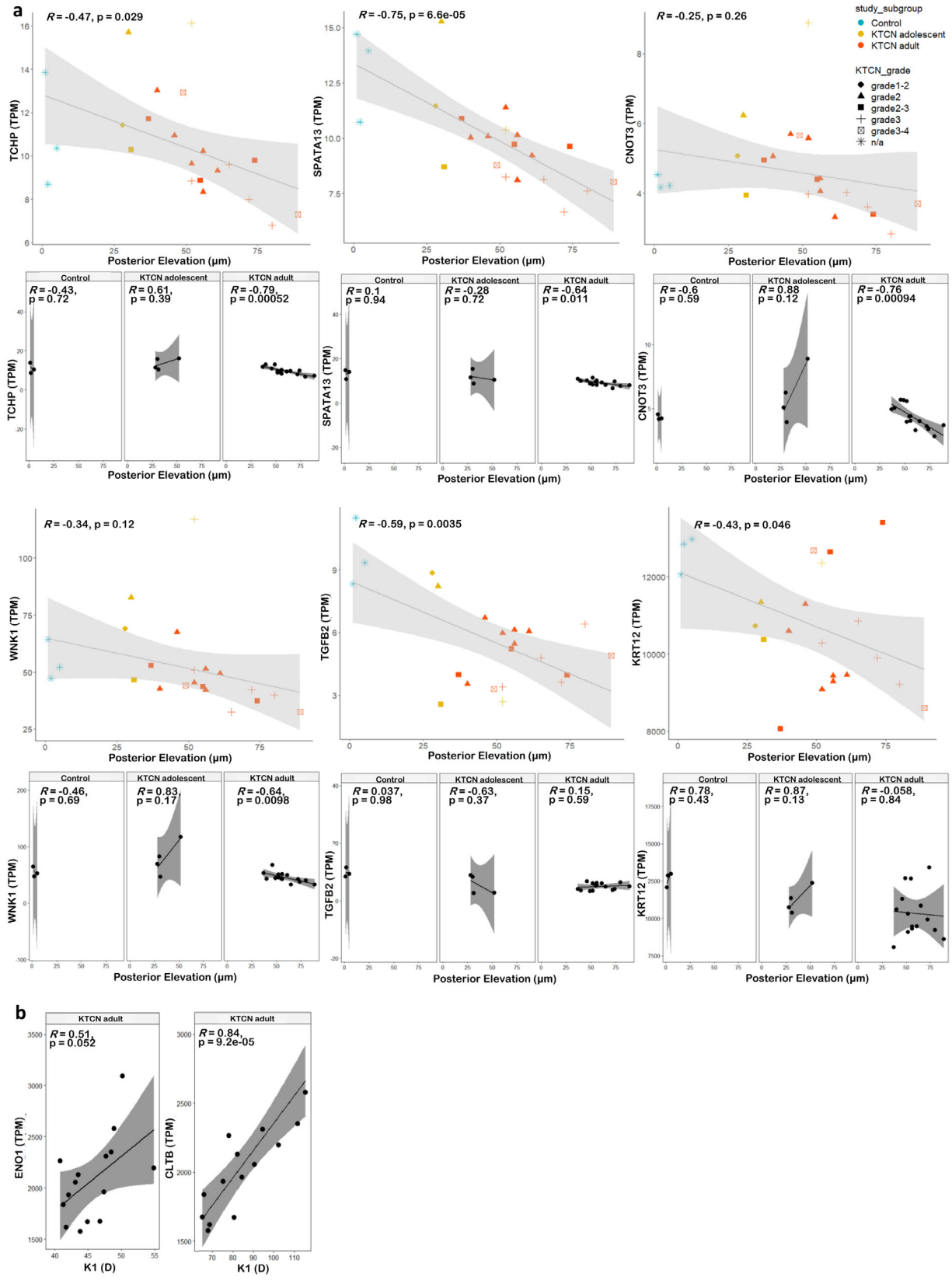

Figure 4. Pearson' correlation results between expression of selected genes, *TCHP*, *SPATA13*, *CNOT3*, *WNK1*, *TGFB2*, *KRT12*, *ENO1*, and *CLTB* (in TPMs), in the *central* CE region and particular clinical features: (**A**) posterior elevation (in micrometers), and (**B**) K1 (in **D**). (**A**) The color of dots and their shape indicate the studied subgroups and the grade of KTCN, respectively. (**B**) Plots show the regression analysis results in the subgroup of adults with KTCN only. Values of regression and statistical significance are presented in the plots.

Investigative Ophthalmology & Visual Science

Table 4. Pathways and Genes of Biological Importance from Transcriptomic (RNA-Seq) and Proteomic (MALDI-TOF/TOF Tandem Mass Spectrometry) Assessments

		KTCN ADULT			*KTCN ADOLESCENT*		
Pathway Module, Pathway	**Study**	***Central* CE Region**	***Middle* CE Region**	***Peripheral* CE Region**	***Central* CE Region**	***Middle* CE Region**	***Peripheral* CE Region**
Cytokine signaling, IFN alpha/beta	RNA-Seq	**IRF9, OAS2, IRF1, IFI27**	**IRF9, OAS2, IFI27, ISG15, HLA-A, HLA-F, STING1**	**IFI27,** ROS1*, ANP32B	**IFI6, IRF9, IRF1**	**IRF9, HLA-H, MX2, MX1**	**IFI27, HLA-H**
	MALDI-MS	**KRT12**		KRT12			
Cytokine signaling, IFN gamma	RNA-Seq	**IRF9, OAS2, IRF1, GBP1,** CES1	**IRF9, OAS2, HLA-A, HLA-F,** FAM220A, CES1	VCAM1*, ROS1*, CES1	**B2M, IRF9, IRF1**	**IRF9, PML, HLA-H, HLA-DRA**	**HLA-H**
	MALDI-MS						
Innate immune system, neutrophil degradation	RNA-Seq	**B4GALT1**	**B4GALT1, STING1, HLA-A**	ADAMTS4*, CXCL1*, LTF*, MMP20*, S100P, MGST1	**PGM2, S100A9, ADAM10, B4GALT1, TICAM2, B2M, SERPINB6**	**S100A9, B4GALT1, HLA-H, STING1, SERPINB6, ALOX5**	**HLA-H, S100A9,** SRP14, EEF2, SNAP23
	MALDI-MS		ABCA13	ABCA13			
Adaptive immune system, class I MHC antigen processing and Presentation	RNA-Seq	**MYD88,** ZBTB16, PRKN	**HLA-A, HLA-F, CD74**	CCDC135*, ANK2*, ASB5*, ZBTB16	**B2M, S100A9,** ZBTB16, FBXO2	**HLA-H, S100A9**	**HLA-H, S100A9,** PAG1, ZBTB16, SNAP23
	MALDI-MS						
Signal transduction, signaling by receptor tyrosine kinases, (including signaling by EGFR)	RNA-Seq	**MT1A**	**ACTB**	PGR*, HGF*, PTN*, NTRK3*, ID4, FGF23, ERBB4, FUS, HNRNPM, PCK1	**CHEK1, ADAM10, STMN1, PPP2R1B, PCSK5,** PCK1	**ID3, PRKCA, NRG2, PDGFA, ID1, HBEGF, ACTB, DUSP7**	PAG1, CHEK1
	MALDI-MS		HSPB1	**PTPRU**			
Signal transduction, signaling by TGFB	RNA-Seq	TGFB2	**CDKN2A**	BMP10*, TGFB2, TCF4	**ITGB6, RBL1,** EMB		EMB
	MALDI-MS		**NDOR1**				
Signal transduction, signaling by WNT	RNA-Seq			AXIN2*, LGR6*, PRKCG*, TBX3*, TRABD2B*, ZEB2, MYEF2, PLCB1, TCF4, PCK1	**H2BC8, H2BC7, H4C13, H2AC17, PPP2R1B,** EMB, PCK1, H2AC18	**PRKCA, WNT9A, H4C12, H4C13**	**H4C12,** PLCB1, EMB
	MALDI-MS			**PTPRU**			
Cell–cell communications, cell–cell junction organization	RNA-Seq	**AJAP1, B4GALT1**	**AJAP1, B4GALT1, ZYX, ACTB**	MAGI2, CDH2*, CDH13*	**PRR4, B4GALT1**	**ZYX, ACTB, KRT7, B4GALT1**	
	MALDI-MS	**ENO1,** KRT7, SHROOM2	**SH3GLB2**	**PTPRU,** WNK4, ENO1	KRT7, SHROOM2	**SHROOM2**	**SHROOM2**
ECM organization, collagen formation	RNA-Seq			MMP20*, COL8A1, **TIMP3**			
	MALDI-MS						
ECM organization, ECM proteoglycans	RNA-Seq	TGFB2, ADARB1	MUSK*, DCN*, TGFB2	**ITGB6**			
	MALDI-MS						

Investigative Ophthalmology & Visual Science

Table 4. Continued

		KTCN ADULT			*KTCN ADOLESCENT*		
Pathway Module, Pathway	**Study**	***Central* CE Region**	***Middle* CE Region**	***Peripheral* CE Region**	***Central* CE Region**	***Middle* CE Region**	***Peripheral* CE Region**
ECM organization, degradation of ECM	RNA-Seq	ADARB1, KLKB1	ADAMTS4*, MMP20*, ELN*, DCN*	**ADAM10**			
	MALDI-MS			ADAM17	ADAM17		ADAM17
ECM organization, integrin cell surface interaction	RNA-Seq	ADARB1	**ZYX**	VCAM1*, ANP32B, COL8A1	**ITGB6**		
	MALDI-MS						
Programmed cell death, apoptosis	RNA-Seq		**DAPK2, TICAM1, CDKN2A**	VIM*	**H1-0, TICAM2, RIPK1**	**TICAM1, H1-0, DAPK2**	HMGB2
	MALDI-MS		HSPB1	**IL1RAP**			
DNA repair, base excision/double-strand breaks repair/mismatch repair	RNA-Seq	**MT1A**	**ISG15, ACTB,** GTF2H2	PLSCR4, CDC45	**H2BC8, H2BC7, H4C13, H2AC17, POLE2, POLQ, CDK1, CHEK1,** H2AC18	**ACTB, H4C12, H4C13**	**H4C12,** CHEK1
	MALDI-MS	TCF20		RMI1	SUMO2	RBBP8	RBBP8
Transcription, positive/negative regulation	RNA-Seq	ZBTB16	**ACTB†, TP53INP2**	ZBTB16*, BLK*, GPC5*, GAD2*, DLX6*, TAL1*, ZNF521*, ANP32B	**H2BC8†, H2BC7†, H4C13†, H2AC17†,** H2AC18†, ZBTB16	**H4C12†, H4C13†**	**H4C12†**
	MALDI-MS	CSDE1, TTBK1	ZBTB4*				
Cell cycle, mitosis/cell cycle checkpoints	RNA-Seq	MAP9	**CDKN2A**	MAP9, GABRG1*, IRGM*, NEFM*, CDK11A, CDC45, CENPM	**AURKA, BUB1B, CHEK1, CENPH, SGO2, BUB1, MAD2L1, SPC24, NUF2, PPP2R1B, CDK1, CENPE, CENPF, CENPA, SKA2, CCNB2, ZWINT, NEK2, CENPJ, MAD2L1, SPC24, CCNB2, RBL1, CENPE, CENPF, CENPA, NCAPG, BUB1B, TOP2A, SGO2, HMMR, ESCO2, POLE2,** EMB, CDKN1C	**PRKCA, KIF2C, CENPA,**	EMB, CHEK1, DMC1, CENPH, CDC45, SMC4, Q9NTJ3, SMC2
	MALDI-MS			RMI1		RBBP8	RBBP8
Developmental biology, Keratinization	RNA-Seq	**KLK13**		KRT26*,KRTAP4-16*, KLK5, KRT13	**KLK13, KRT24, KRT8**	**KLK13, KRT7, KRT24,** SPINK5, KRT6A	**KRT24,** SPINK5, KRT6A
	MALDI-MS	**KRT7, KRT12**	KRT3	KRT7, KRT12	**KRT78**	**KRT78**	

Presented are genes/proteins with upregulated (FC of ≥1.5) or downregulated (FC of ≤0.5) expression/protein levels in the particular CE regions of adults or adolescents with KTCN, attributed to biological pathways revealed as significant in pathway enrichment and hallmarks analyses. In RNA-Seq we performed the differential expression analysis using limma package. Additionally, we calculated the expression of genes [with a mean expression level of ≥1 transcript per million (TPM) from a particular pathway gene set, and defined it as significant based on the following cutoffs: $P \leq 0.05$ (*t* test) and FC of ≥1.5 or ≤0.5. For MALDI-TOF/TOF tandem mass spectrometry data analyses, we implemented mathematical algorithms (quick classifier [QC] and genetic algorithm [GA]) regarding CE samples of adults with KTCN and controls, whereas discriminative peaks for CE samples of adolescents with KTCN (compared with controls) were calculated in JASP Software. Extended list of pathways and genes of biological importance is presented in Supplementary Table S10.

MALDI-MS, MALDI-TOF/TOF Tandem Mass Spectrometry.

Bold text indicates the upregulated expression/level of gene/protein.

* Differentially expressed genes revealed using limma package.

† Genes involved in the regulation of gene expression by methylation.

Investigative Ophthalmology & Visual Science

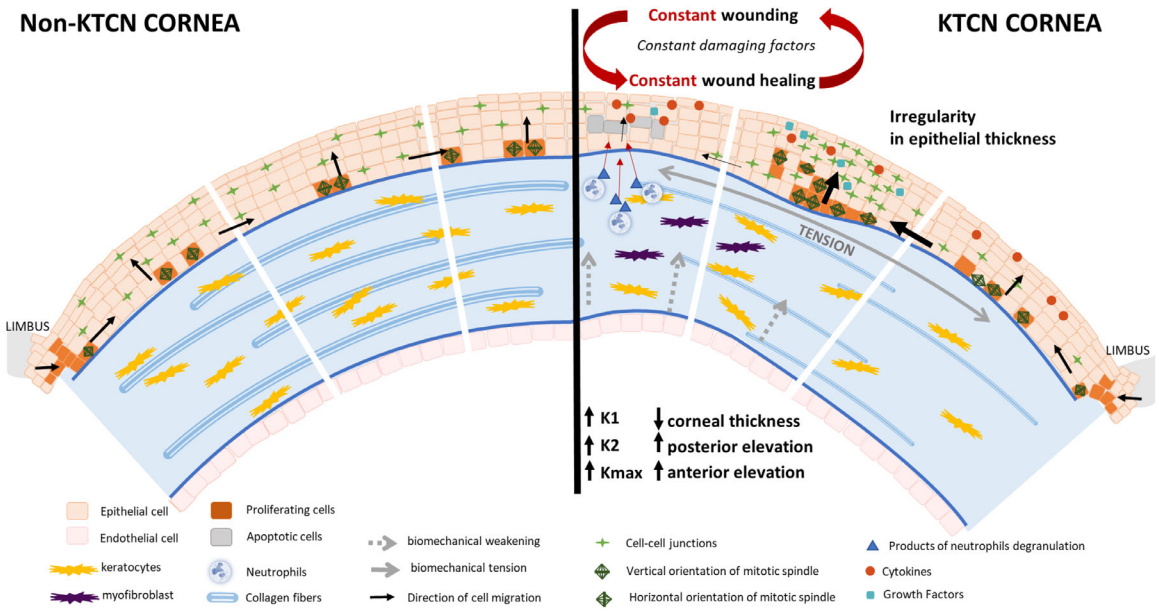

Figure 5. Hypothetical mechanism of CE remodeling in KTCN (white vertical lines indicate boundaries of the corneal *topographic* regions). In KTCN, the physiological conditions of cornea biomechanics, dynamic interactions of cells, and homeostasis of cytokines and growth factors are disturbed. The progressive biomechanical weakening of the cornea, being a consequence of changes in collagen fibers and other elements of extracellular matrix in the stroma, contributes to the additional tension of the cornea and results in increased posterior elevation, anterior elevation, and keratometry as well as the decreased corneal thickness. The CE remodeling is triggered by constant wounding stimulated by both eye rubbing and dysregulated immune responses. Simultaneously, the released growth factors, cytokines, and products of neutrophil degranulation induce apoptosis, mesenchymal differentiation, and wound healing. Additional dysregulation of the cell migration process causes a constant, instead of a transient, wound healing state. The initially protective inflammation contributes to the progressive corneal weakening manifested by cone formation, which constitutes the most susceptible zone for further corneal injuries. Intensified cell migration from the *peripheral* to the *middle topographic* region of CE and simultaneously reduced migration of cells from *middle* to *central topographic* region, modifications of mitotic spindle' orientation from horizontal to vertical, as well as changes in cell cycle checkpoints, DNA repair, and apoptosis cause the accumulation of cells and increased epithelial thickness in the *middle topographic* region of CE. Concurrently, these factors lead to decrease in the cell number and epithelial thickness in the *central topographic* region.

with KTCN, the relationships with clinical outcomes showed the following expression products correlating with K1: *ENO1* (K1; R = 0.51; $P = 0.52$) and *CLTB* (K1; R = 0.84; $P = 9.2e\text{-}05$) (Fig. 4B).

Pathways and Genes of Biological Importance: Abnormal Immune Responses, ECM Organization, and Cell Cycle, and Mechanisms of CE Remodeling

Results of the transcriptomic and proteomic data consolidation are presented as 17 pathways' branches in Table 4, and in the extended version of this table in Supplementary Table S10 (28 pathways' branches). Indicated pathways correspond with Supplementary Figure S6, as a visualization of networks for particular *topographic* regions of the CE. Deregulation of biological pathways such as IFN alpha/beta signaling, IFN gamma signaling, and neutrophil degranulation was revealed. Moreover, the decrease in the elements of the ECM (integrin cell surface interaction, collagen formation, and proteoglycans) was disclosed. Cell cycle and transcription, as well as DNA repair, were the processes substantially upregulated in the *central* and *middle* CE regions of adolescent patients compared with both adults with KTCN and controls. Combined data regarding the selected distinguishing pathways, together with the identified alternations are presented in Supplementary Figure S7, and the remaining results are compiled in Supplementary Figure S8. Additionally, the discovered high-impact and missense variants revealed in the four youngest patients with KTCN in our study group, assumed to contribute to the molecular picture of KTCN discussed here, in particular CE, are presented in Supplementary Table S11.

The hypothetical mechanism of formation of the CE *doughnut*, embracing elements of the corneal biomechanical weakening, dysregulation of immune responses, and altered cell migration, resulting in constant wounding and wound healing of CE and remodeling of CE, are presented and described in detail in Figure 5.

Discussion

Thus far, pathological changes in the cornea during KTCN development, leading to keratoconic cone formation, have been explained frequently by the incorrect arrangement of the stroma, and thus impairment of its physiological function.[48–50] To compliment previous, solely clinical findings, we delved into the corneal *topographic* regions of the KTCN cornea.

Discriminating Clinical Features, Epithelial *Doughnut*, and Corneal *Topographic* Regions

In line with previously reported epithelial thickness irregularity and asymmetry, as discriminating factors between keratoconic and healthy eyes,[51,52] we found a decrease in the

average epithelial thickness at the corneal apex in adults and adolescents with KTCN compared with unaffected eyes. Our finding of the most common cone locations in central temporal and inferior temporal, in both adults and adolescents with KTCN, corresponds with previously described keratoconic cones decentered to the inferior temporal location.[51,53]

On the maps of the epithelial thickness of our adult and adolescent patients with KTCN, the central cone, which is the thinnest region, was found to be surrounded by a thickened *middle* region of full- or open-ring shape, which has been reported and named as an epithelial *doughnut*.[21,51,53] Despite that well-known pattern, aspects of clinical, morphological, and molecular abnormalities in the CE of patients with KTCN and especially in the *topographic* regions of the CE have not been evaluated extensively. These days, first experiments are being performed based on the separation of corneal layers[54,55] or single-cell approaches[22] toward a more detailed assessment, but the design of these studies have not reflected the KTCN-specific *doughnut* pattern.

Moving toward unraveling the novel mechanistic aspects of KTCN development in the CE, we designated *central*, *middle*, and *peripheral topographic* regions of the CE based on the CE thickness irregularity observed in adults and adolescents with KTCN, and we compared the obtained data with the corresponding *topographic* regions of the CE in controls to determine biological diversity. To date, there was no KTCN study assessing three distinct *topographic* regions of the CE based on the CE thickness maps. While in two studies the separation of two *topographic* regions, the conical and nonconical zones has been implemented, the distinctive pattern of the epithelial *doughnut* in KTCN has not been evaluated.[54,56] Molecular analyses restricted to selected genes,[56] no details of the clinical examination of control individuals,[56] and lack of separation of control corneas into the two examined cone and non-cone zones[54] were additional limitations of these studies.

Morphological Diversity of the CE *Topographic* Regions

Morphological examination of the CE samples of controls showed a balance in the number of cells, confirmed by the nuclei number measurements, between the particular *topographic* regions. In contrast with controls, in the CE samples of patients with KTCN, an imbalance in the number and size of nuclei, with the greatest increase of number and decrease of size of nuclei in the *middle* CE region was observed. As predicted, a decrease in nuclei number in the *central* region of the CE was found. Morphological alterations were also visible in the *peripheral* CE region, somewhat reminiscent of the changes observed in the *middle* region, and in particular as an increase in the number and a decrease in the size of the cells. The identified features of the *peripheral* CE region of patients with KTCN were not detectable in the epithelial thickness mapping.

Deregulated Immune Responses in KTCN CE

Since 2017, we have been constantly confirming the hypothesis that the deregulated pathways, and not the disturbance of the expression of individual genes, constitute the molecular signature of KTCN.[31,42,43] Consequently, here, by consolidation of multi-omic data, we demonstrated the overall upregulation in IFNs alpha/beta and gamma signaling in both evaluated subgroups of patients with KTCN, which corresponds with previous reports on cytokines profile in the tear fluid.[57,58] However, in addition to the IFNs, we have found dysregulation of antigen processing and presentation pathway and allograft rejection hallmark. Additionally, the molecular changes found on genomic level indicate a more complex inflammatory background in KTCN as previously anticipated (Jaskiewicz et al. 2022, unpublished data). The presence of variants in genes involved in antigen processing and presentation (Jaskiewicz et al. 2022, unpublished data), together with the eye rubbing and allergy, could contribute to chronic corneal epithelial injury and trigger constant stimulation of wound healing in KTCN, as previously suggested.[59] In line with these results, here we presented the decreased level of clusterin (CLU) protein in the *peripheral* region of CE, which was previously demonstrated to be repressed during closure of wounds in tissue-engineered human cornea,[60] and the increased level of keratin 12 (KRT12) protein in the *central* region of CE, earlier reported as an effect of repairing response after injury.[61]

Impaired Wound Healing Process in KTCN CE

Because of constant wounding and stimulation of wound healing in KTCN,[59] and prolonged inflammation leading even to corneal scarring and vision impairment,[62] a properly functioning repair mechanism is crucial to provide homeostasis in CE.[63] Here, the expression of genes involved in response to wounding (*ITGB1*, *LOX*, *CD44*, *PECAM1*, *DST*, *DCN*, *B4GALT1*, *WNT5A*, and *TNFSRF12A*) was identified to be upregulated in the *central* and *middle* CE regions, but downregulated in the *peripheral* region of KTCN CE, suggesting that this process is differentially altered, depending on the region. Also, by combining the clinical and molecular data, we revealed the correlation between posterior corneal elevation and expression of the *WNK1* gene, which was previously found to contribute to the healing of corneal wounds in the tissue-engineered human cornea.[64] Additionally, in the *peripheral* region of CE of adults with KTCN, we found downregulated expression of the *HGF* gene, which could explain dysregulation of the migration of epithelial cells[65] and corneal epithelial wound healing.[66] Moreover, a previously not reported in the CE pathology aspect concerning the neutrophil degranulation pathway was found to be upregulated in the *central* and *middle* regions of the CE, but downregulated in the *peripheral* region of the CE of adults with KTCN. The role of neutrophils in stromal wound healing has been established previously.[59,67] At this point, we hypothesize that the observed dysregulation may be an effect of the interplay of stromal and epithelial wound healing rather than the infiltration of neutrophils into the CE from the stroma. Moreover, the revealed single high-impact sequence variants (*CEP290*, *MMRN1*, and *FN1*), and missense variants (*PECAM1*, *VWF*, *CD109*, *HRG*, *TLN1*, *HPSE*, *EPO*, *SIGLEC10*, *DOCK8*, *ERBB3*, and *AP3B1*) in CE samples of adolescents with KTCN (Jaskiewicz et al. 2022, unpublished data) confirm the importance of this supposition, as may have contributed to this molecular dysregulation of wound healing, although we have not determined their impact.

Because wound healing induces cell migration,[68] its efficacy could be also affected by the epithelial–mesenchymal transition and cell–cell communications, including the

cell–cell junctions and cell–ECM interactions.[63] In the *peripheral* region of CE of adults with KTCN, we found decreased expression of fibronectin (*FNDC1*), previously described as contributing to the scaffold of ECM and reported to be a mesenchymal marker.[69] Additionally, the hallmark of epithelial–mesenchymal transition was recognized to be elevated in the *central* and *middle* CE regions of adults with KTCN and in the *central* CE region of adolescents with KTCN. Regarding the aspect of the cell–cell communications, we revealed the upregulated pathways of tight and adherent junctions' organization in the *middle* CE region of adults with KTCN. Also, the claudin-related genes' expression was mostly increased in the *middle* CE region of adults with KTCN. Given both pro-proliferative and antiapoptotic functions of these genes,[70] this factor may explain the observable morphological pattern of CE in the *middle* CE region in patients with KTCN.

The cell–ECM interdependencies are another recognized, crucial element of cell migration.[71] The disruption of the organization of ECM was one of the features previously revealed in the transcriptome or pathways analysis in whole-thickness corneas,[31,43] cultured stromal cells from KTCN corneas,[72] and now in CE of patients with KTCN. Here, the downregulation of integrin cell surface interactions, collagen formation, ECM proteoglycans, and degradation of the ECM in the *peripheral* CE region of patients with KTCN was revealed as the most significant finding. Moreover, in the aspect of integrins-mediated cell adhesion to the ECM substantial overlap between transcriptomic and genomic findings (Jaskiewicz et al. 2022, unpublished data), which emphasize the importance of these results. Summarizing here, the revealed impaired ECM organization and cell–cell communication in the *central* and *middle* CE regions of adults with KTCN might cause the decreased epithelial cell motility in these regions through deregulation of cells migration, as previously found in rabbit normal corneas,[63] and corneal epithelial cell line.[73] Downregulated expression of cadherin *CDH13* taken together with the decreased levels of ENO1 protein (as elements of cell adherent junctions) and WNK4 protein (as an element of tight junctions) in the *peripheral* region, could intensify cell migration from the *peripheral* to *middle* CE region, leading to an accumulation of cells in the *middle* region of the CE and forming the aforementioned *doughnut* pattern. Also, based on the obtained results, we take into consideration that the *doughnut* pattern may result from an alteration in the cells' proliferation and cell cycle progression through the upregulation of apoptosis, G2M checkpoints, and DNA repair pathways in the *central* and *peripheral* CE regions. Additionally, in the aspects of cell proliferation, we found the upregulated hallmark of the mitotic spindle in all the *topographic* regions of adults with KTCN and in the *central* region of adolescents with KTCN. Previously, the vertical and horizontal orientation of the mitotic spindle has been described in normal CE as a feature possibly influencing both cell migration and cell division.[74] Delving into the genetic aspects we identified high impact variants in *INSC* gene in CE samples of adolescents with KTCN (Jaskiewicz et al. 2022, unpublished data), which is involved in spindle orientation during mitosis.[75] However, we have no evidence to verify the observable increase in the number of cells in the *middle* region compared with the *central* and *peripheral* region of CE, and to confirm whether it is a result of an increased proliferation of cells or their arrest at a given stage of the cell cycle.

Dysregulated Gender-related Pathways

We also focus on sex hormones, which were reported as the players in epithelial–mesenchymal transition,[76] cytoskeleton modulators,[77] and transcriptional activators.[78,79] The influence of gender on expression of more than 600 genes in CE of unaffected individuals[80] and patients with KTCN[55] was previously reported. Because such gender dependence embraces the genes responsible for cell growth, migration, and proliferation, we limited our further analyses to males instead of discriminating off all genes with gender-dependent expression. Regardless of the fact that female patients were excluded from molecular analyzes, we observed disturbances in hormone-related pathways, with the activated PKN1 stimulates transcription of androgen receptor regulated genes KLK2 and KLK3 pathway as the most upregulated in the CE of patients with KTCN.

Impact of the Stage of Progression in KTCN, Indicators, and Translational Relevance

Because the same morphological abnormalities of the CE were demonstrated in adults and adolescents with KTCN, to differentiate these patients' subgroups the transcriptomic and proteomic features together with clinical findings were evaluated, also in direction of identification of KTCN-specific indicators. In the comparison between adolescents and adults, the enrichment in transcription and mitosis pathways in adolescents were revealed, whereas other features were specific for adults with KTCN, including the ECM organization, epithelial–mesenchymal transition, inflammatory response, and TGF-β signaling. We noticed significantly higher values of posterior elevation in adults with KTCN in comparison with adolescents with KTCN.

Although the difference in the posterior elevation between adults with KTCN and adolescents with KTCN may be explained by the CXL procedure performed before the advanced stage of pediatric KTCN owing to the high risk of rapid progression,[81–83] the clinical–transcriptomic correlations found in this study allowed us to point to the KTCN indicators. Because posterior elevation has been reported as a strong discriminating factor of normal and KTCN eyes allowing the diagnosis before a patient becomes symptomatic,[84] and we pointed to the correlations of clinical and transcriptomic elements, the latter might be of translational relevance. For example, we can apply a noninvasive method, an impression cytology, to harvest CE cells. Here, we demonstrated a significant negative correlation between the expression of proapoptotic *TCHP*,[85] regulating cell migration *SPATA13*,[86] promitotic *CNOT3*,[87] wound healing–related *WNK1*,[64] cells' growth affecting *TGFB2*,[88] involved in CE organization *KRT12*,[89] and the value of posterior corneal elevation. We also found other correlations of clinical–transcriptome elements that, however, do not differentiate adults and adolescents with KTCN. The expression of *ENO1* involved in allergic responses[90] and *CLTB* involved in clathrin-dependent endocytosis[91] showed a strong positive correlation with the K1 value.

Mechanism of CE Remodeling in KTCN

Finally, summarizing all the findings, we propose the mechanism of cell and molecule migration in the three *topographic* regions leading to CE remodeling. Under physiological conditions, the proper dynamics of cells, cytokines,

Investigative Ophthalmology & Visual Science

growth factors, and lipids between the epithelium and the stroma promote epithelial integrity and protective inflammation, as well as limiting corneal fibrosis.[92,93] In KTCN, the physiological conditions of cornea biomechanics, dynamic interactions of cells, and homeostasis of cytokines and growth factors are disturbed. In KTCN, the progressive biomechanical weakening of the cornea, being a consequence of changes in collagen fibers and other elements of extracellular matrix in the stroma, contributes to the additional tension of the cornea and results in increased posterior elevation, anterior elevation, and keratometry, as well as decreased corneal thickness.[56,94] The contribution of CE to the overall biomechanical properties of the cornea has been confirmed in studies showing the association between corneal stiffness parameters A1 and corneal epithelial thickness[61] or even removal of epithelium.[95] Interestingly, in KTCN the CE is able rebuild in response to underlying stromal irregularities, allowing the creation of a symmetrical optical surface.[53,96] This remodeling is triggered by constant wounding stimulated by both eye rubbing and dysregulated immune responses. Disturbance of the immunological homeostasis may cause stimulation of the keratocyte into myofibroblast, due to a release of TGF-β2 from CE cells,[97] whereas loosing of TNF-α expression in stromal cells results in thinning of CE.[92] The released growth factors, cytokines, and products of neutrophil degranulation induce apoptosis, mesenchymal differentiation, and wound healing. Nevertheless, additional dysregulation of the cell migration process causes a constant, instead of a transient, wound healing state. Initially protective inflammation contributes to the progressive corneal weakening manifested by keratoconic cone formation, which is the most susceptible zone for further injuries. Intensified cell migration from the *peripheral* to the *middle topographic* region of CE and simultaneously decreased migration of cells from *middle* to *central topographic* region and modification of mitotic spindle orientation from horizontal to vertical, as well as changes in cell cycle checkpoints, DNA repair, and apoptosis, cumulatively cause the accumulation of cells and increased epithelial thickness in the *middle topographic* region of CE. Concurrently, these factors lead to a decrease in the cell number and epithelial thickness in the *central topographic* region.

Taking into account the multiple molecular and isolated clinical differences between adults and adolescents with KTCN, the disease duration and the likely sequence of changes in the layers of the cornea during disease development (changes in the posterior surface of the cornea are the earliest observed feature of KTCN[13]), we concluded that the recognized correlations of posterior elevation and transcriptome features might have translational relevance. In our study, the *doughnut* pattern of the CE was observed in both subgroups of patients with KTCN; therefore, we assume that morphological compensation of CE occurs quickly after the first lesions of the posterior surface of the cornea, which is in line with previous data.[1,13] Subsequently, further progression of KTCN in adults, as the increased steepening of posterior surface curvature leading to aggravating of cornea's properties, results in increased biomechanical and molecular interactions between the stroma and epithelium.

We are aware of the limitations of our study. It is not possible to obtain the CE from healthy individuals for research purposes; this is why patients with mild myopia undergoing the PRK surgery as non-KTCN controls were ascertained, as previously practiced by Pahuja et al.,[56] You et al.,[55] and Karolak et al.[42] Moreover, obtaining the CE samples from the control individuals toward transcriptomic assessment was especially challenging, because this type of material could be collected during a PRK procedure only, which nowadays is rarely performed, having been replaced with the newer techniques of vision correction in which the CE is not removed. The PRK procedure is performed only in adult individuals and this fact also results in the lack of age-matched controls in analyzes embracing adolescents with KTCN. We were able to collect only the samples of CE; therefore, our suggestions regarding the interaction between CE and subsequent corneal layers are based only on clinical data and need to be verified in further study involving both CE and stroma samples. More men than women were identified in the examined study subgroups, which is in line with the predominance of male patients among 110 individuals undergoing the CXL procedure in 2020 through 2022 in the Optegra Clinic (19 female and 91 male patients, unpublished data, Dr. Maleszka-Kurpiel, personal communication), and with other reports.[98–100]

To conclude, we found characteristic and distinguishing features for particular CE *topographic* regions in KTCN, pointing to their involvement in the stated mechanism of CE remodeling. The revealed changes in the CE molecular profiles are a consequence of the progression of KTCN rather than the cause of the disease. The presented molecular, morphological, and clinical evidence supports our hypotheses regarding the impaired wound healing in KTCN, the disturbed epithelial–stromal interactions, and biomechanical compensation of the posterior corneal surface. Importantly, the clinical–molecular indicators identified here are the measurable findings related to KC pathogenesis.

Acknowledgments

The authors are grateful to the director and the team of the Optegra Eye Health Care Clinic in Poznan, Poland, for enabling biological sampling and assisting in patient recruitment and clinical evaluation.

Special thanks to Pawel Stankiewicz for his assistance in the whole genome sequencing.

Supported by National Science Centre in Poland, Grants 2018/31/B/NZ5/03280 (to MG) and 2021/41/B/NZ5/02245 (to MG).

Next-generation sequencing was performed thanks to Genomics Core Facility CeNT UW using NovaSeq 6000 platform financed by the Polish Ministry of Science and Higher Education (decision no. 6817/IA/SP/2018 of 2018-04-10).

Author Contributions: KJ participated in research design, sample collection, and patient surveys; performed sample preparations toward RNA-Seq, MALDI-TOF/TOF Tandem Mass Spectrometry, and morphological experiments; participated in RNA-Seq experiments; participated in bioinformatics analyses; figures and tables preparation; participated in the transcriptomic, proteomic, morphological and clinical data interpretation; performed biological interpretation of the results; wrote the manuscript. MMK performed patients' recruitment and clinical evaluation; facilitated sample collection; performed the clinical data interpretation; participated in the transcriptomic, proteomic, morphological and clinical data interpretation; performed biological interpretation of the results; wrote the manuscript. EM participated in the setup of MALDI-TOF/TOF Tandem Mass Spectrometry experiments and proteomic data interpretation; performed MALDI-TOF/TOF Tandem Mass Spectrometry experiments, MALDI-TOF/TOF Tandem Mass

Spectrometry data analysis, preparation of MALDI-TOF/TOF Tandem Mass Spectrometry figures, and tables. MK performed setup of bioinformatics pipeline, bioinformatics analyses of transcriptomic data; preparation of figures and tables. MR performed RNA-Seq experiments and transcriptomic data interpretation. RM: participated in the setup of morphological assessment and data interpretation. RP participated in the transcriptomic data interpretation. JM participated in the setup of MALDI-TOF/TOF Tandem Mass Spectrometry experiments and proteomic data interpretation. MG performed research design; secured research funding; participated in the transcriptomic, proteomic, morphological, and clinical data interpretation; performed biological interpretation of the results; and edited the manuscript.

All authors contributed to critical revisions and approved the final manuscript.

Disclosure: **K. Jaskiewicz**, None; **M. Maleszka-Kurpiel**, None; **E. Matuszewska**, None; **M. Kabza**, None; **M. Rydzanicz**, None; **R. Malinowski**, None; **R. Ploski**, None; **J. Matysiak**, None; **M. Gajecka**, None

References

1. Reinstein DZ, Archer TJ, Urs R, Gobbe M, RoyChoudhury A, Silverman RH. Detection of keratoconus in clinically and algorithmically topographically normal fellow eyes using epithelial thickness analysis. *J Refract Surg*. 2015;31(11):736–744, doi:10.3928/1081597X-20151021-02.
2. Ferrari G, Rama P. The keratoconus enigma: a review with emphasis on pathogenesis. *Ocul Surf*. 2020;18(3):363–373, doi:10.1016/j.jtos.2020.03.006.
3. Hashemi H, Heydarian S, Hooshmand E, et al. The prevalence and risk factors for keratoconus: a systematic review and meta-analysis. *Cornea*. 2020;39(2):263–270, doi:10.1097/ICO.0000000000002150.
4. Iwaszkiewicz E. [Keratoconus. I. Various epidemiologic data]. *Klin Oczna*. 1989;91(7-9):208–209.
5. Agency for Health Technology Assessment and Tariffs; 2015. Polish Health Problem Card. Recommendation No. 93/2015 of 1 December 2015 of the President of the Agency for Health Technology Assessment and Tariffs on the qualification of the service "Cross-linking keratoconus surgery (X-linking)" as a guaranteed hospital treatment service. Available at: https://bipold.aotm.gov.pl/assets/files/zlecenia_mz/2015/018/REK/RP_93_2015_%20X-linking.pdf.
6. Najmi H, Mobarki Y, Mania K, et al. The correlation between keratoconus and eye rubbing: a review. *Int J Ophthalmol*. 2019;12(11):1775–1781, doi:10.18240/ijo.2019.11.17.
7. Roy S, Yadav S, Dasgupta T, Chawla S, Tandon R, Ghosh S. Interplay between hereditary and environmental factors to establish an in vitro disease model of keratoconus. *Drug Discov Today*. 2019;24(2):403–416, doi:10.1016/j.drudis.2018.10.017.
8. Bykhovskaya Y, Rabinowitz YS. Update on the genetics of keratoconus. *Exp Eye Res*. 2021;202:108398, doi:10.1016/j.exer.2020.108398.
9. Karolak JA, Gajecka M. Genomic strategies to understand causes of keratoconus. *Mol Genet Genomics*. 2017;292(2):251–269, doi:10.1007/s00438-016-1283-z.
10. Loukovitis E, Sfakianakis K, Syrmakesi P, et al. Genetic aspects of keratoconus: a literature review exploring potential genetic contributions and possible genetic relationships with comorbidities. *Ophthalmol Ther*. 2018;7(2):263–292, doi:10.1007/s40123-018-0144-8.
11. Moussa S, Grabner G, Ruckhofer J, Dietrich M, Reitsamer H. Genetics in keratoconus— what is new? *Open Ophthalmol J*. 2017;11:201–210, doi:10.2174/1874364101711010201.
12. Silverman RH, Urs R, RoyChoudhury A, Archer TJ, Gobbe M, Reinstein DZ. Combined tomography and epithelial thickness mapping for diagnosis of keratoconus. *Eur J Ophthalmol*. 2017;27(2):129–134, doi:10.5301/ejo.5000850.
13. Sedaghat MR, Momeni-Moghaddam H, Roberts CJ, Maddah N, Ambrósio R, Hosseini SR. Corneal biomechanical parameters in keratoconus eyes with abnormal elevation on the back corneal surface only versus both back and front surfaces. *Sci Rep*. 2021;11(1):11971, doi:10.1038/s41598-021-91263-7.
14. Gain P, Jullienne R, He Z, et al. Global survey of corneal transplantation and eye banking. *JAMA Ophthalmol*. 2016;134(2):167–173, doi:10.1001/jamaophthalmol.2015.4776.
15. MM Al-Mohaimeed. Combined corneal CXL and photorefractive keratectomy for treatment of keratoconus: a review. *Int J Ophthalmol*. 2019;12(12):1929–1938, doi:10.18240/ijo.2019.12.16.
16. Meek KM, Hayes S. Corneal cross-linking— a review. *Ophthalmic Physiol Opt*. 2013;33(2):78–93, doi:10.1111/opo.12032.
17. Raiskup-Wolf F, Hoyer A, Spoerl E, Pillunat LE. Collagen crosslinking with riboflavin and ultraviolet-A light in keratoconus: long-term results. *J Cataract Refract Surg*. 2008;34(5):796–801, doi:10.1016/j.jcrs.2007.12.039.
18. Wollensak G. Crosslinking treatment of progressive keratoconus: new hope. *Curr Opin Ophthalmol*. 2006;17(4):356–360, doi:10.1097/01.icu.0000233954.86723.25.
19. Naderan M, Jahanrad A, Balali S. Histopathologic findings of keratoconus corneas underwent penetrating keratoplasty according to topographic measurements and keratoconus severity. *Int J Ophthalmol*. 2017;10(11):1640–1646, doi:10.18240/ijo.2017.11.02.
20. Sykakis E, Carley F, Irion L, Denton J, Hillarby MC. An in depth analysis of histopathological characteristics found in keratoconus. *Pathology (Phila)*. 2012;44(3):234–239, doi:10.1097/PAT.0b013e3283511b42.
21. Wang Q, Lim L, Lim SWY, Htoon HM. Comparison of corneal epithelial and stromal thickness between keratoconic and normal eyes in an Asian population. *Ophthalmic Res*. 2019;62(3):134–140, doi:10.1159/000500313.
22. Collin J, Queen R, Zerti D, et al. A single cell atlas of human cornea that defines its development, limbal progenitor cells and their interactions with the immune cells. *Ocul Surf*. 2021;21:279–298, doi:10.1016/j.jtos.2021.03.010.
23. Rubelowski AK, Latta L, Katiyar P, et al. HCE-T cell line lacks cornea-specific differentiation markers compared to primary limbal epithelial cells and differentiated corneal epithelium. *Graefes Arch Clin Exp Ophthalmol*. 2020;258(3):565–575, doi:10.1007/s00417-019-04563-0.
24. Shinde V, Hu N, Renuse S, et al. Mapping keratoconus molecular substrates by multiplexed high-resolution proteomics of unpooled corneas. *OMICS J Integr Biol*. 2019;23(11):583–597, doi:10.1089/omi.2019.0143.
25. Sridhar M. Anatomy of cornea and ocular surface. *Indian J Ophthalmol*. 2018;66(2):190, doi:10.4103/ijo.IJO_646_17.
26. JASP Team 2022. JASP Team (2022). JASP (Version 0.16.3) [Computer software]. Published online 2022. Available at: https://jasp-stats.org/.
27. Brittingham S, Tappeiner C, Frueh BE. Corneal cross-linking in keratoconus using the standard and rapid treatment protocol: differences in demarcation line and 12-month outcomes. *Invest Ophthalmol Vis Sci*. 2014;55(12):8371–8376, doi:10.1167/iovs.14-15444.

Investigative Ophthalmology & Visual Science

28. Raiskup F, Spoerl E. Corneal crosslinking with riboflavin and ultraviolet A. Part II. Clinical indications and results. *Ocul Surf*. 2013;11(2):93–108, doi:10.1016/j.jtos.2013.01.003.
29. Wollensak G, Spoerl E, Seiler T. Riboflavin/ultraviolet-a-induced collagen crosslinking for the treatment of keratoconus. *Am J Ophthalmol*. 2003;135(5):620–627, doi:10.1016/s0002-9394(02)02220-1.
30. Ganesh S, Brar S, Patel U. Comparison of ReLEx SMILE and PRK in terms of visual and refractive outcomes for the correction of low myopia. *Int Ophthalmol*. 2018;38(3):1147–1154, doi:10.1007/s10792-017-0575-6.
31. Kabza M, Karolak JA, Rydzanicz M, et al. Collagen synthesis disruption and downregulation of core elements of TGF-β, Hippo, and Wnt pathways in keratoconus corneas. *Eur J Hum Genet EJHG*. 2017;25(5):582–590, doi:10.1038/ejhg.2017.4.
32. Kabza M, Karolak JA, Rydzanicz M, et al. Multiple differentially methylated regions specific to keratoconus explain known keratoconus linkage loci. *Invest Ophthalmol Vis Sci*. 2019;60(5):1501, doi:10.1167/iovs.18-25916.
33. Stein LD. Using the Reactome database. *Curr Protoc Bioinforma*. 2004;7(1); Chapter 8:Unit 8.7, doi:10.1002/0471250953.bi0807s7.
34. Wu D, Smyth GK. Camera: a competitive gene set test accounting for inter-gene correlation. *Nucleic Acids Res*. 2012;40(17):e133, doi:10.1093/nar/gks461.
35. Liberzon A, Birger C, Thorvaldsdóttir H, Ghandi M, Mesirov JP, Tamayo P. The Molecular Signatures Database (mSigDB) hallmark gene set collection. *Cell Syst*. 2015;1(6):417–425, doi:10.1016/j.cels.2015.12.004.
36. Szklarczyk D, Gable AL, Nastou KC, et al. The STRING database in 2021: customizable protein-protein networks, and functional characterization of user-uploaded gene/measurement sets. *Nucleic Acids Res*. 2021;49(D1):D605–D612, doi:10.1093/nar/gkaa1074.
37. Gillespie M, Jassal B, Stephan R, et al. The reactome pathway knowledgebase 2022. *Nucleic Acids Res*. 2022;50(D1):D687–D692, doi:10.1093/nar/gkab1028.
38. Mi H, Muruganujan A, Ebert D, Huang X, Thomas PD. PANTHER version 14: more genomes, a new PANTHER GO-slim and improvements in enrichment analysis tools. *Nucleic Acids Res*. 2019;47(D1):D419–D426, doi:10.1093/nar/gky1038.
39. Rodchenkov I, Babur O, Luna A, et al. Pathway Commons 2019 Update: integration, analysis and exploration of pathway data. *Nucleic Acids Res*. 2020;48(D1):D489–D497, doi:10.1093/nar/gkz946.
40. Csabai L, Fazekas D, Kadlecsik T, et al. SignaLink3: a multi-layered resource to uncover tissue-specific signaling networks. *Nucleic Acids Res*. 2022;50(D1):D701–D709, doi:10.1093/nar/gkab909.
41. Licata L, Lo Surdo P, Iannuccelli M, et al. SIGNOR 2.0, the SIGnaling Network Open Resource 2.0: 2019 update. *Nucleic Acids Res*. 2020;48(D1):D504–D510, doi:10.1093/nar/gkz949.
42. Karolak JA, Ginter-Matuszewska B, Tomela K, et al. Further evaluation of differential expression of keratoconus candidate genes in human corneas. *PeerJ*. 2020;8:e9793, doi:10.7717/peerj.9793.
43. Karolak JA, Gambin T, Rydzanicz M, et al. Accumulation of sequence variants in genes of Wnt signaling and focal adhesion pathways in human corneas further explains their involvement in keratoconus. *PeerJ*. 2020;8:e8982, doi:10.7717/peerj.8982.
44. Li H. Aligning sequence reads, clone sequences and assembly contigs with BWA-MEM. arXiv:1303.3997. Published online 2013, doi:10.48550/ARXIV.1303.3997.
45. Tarasov A, Vilella AJ, Cuppen E, Nijman IJ, Prins P. Sambamba: fast processing of NGS alignment formats. *Bioinforma Oxf Engl*. 2015;31(12):2032–2034, doi:10.1093/bioinformatics/btv098.
46. Rimmer A, Phan H, Mathieson I, et al. Integrating mapping-, assembly- and haplotype-based approaches for calling variants in clinical sequencing applications. *Nat Genet*. 2014;46(8):912–918, doi:10.1038/ng.3036.
47. McLaren W, Gil L, Hunt SE, et al. The Ensembl variant effect predictor. *Genome Biol*. 2016;17(1):122, doi:10.1186/s13059-016-0974-4.
48. Alkanaan A, Barsotti R, Kirat O, Almubrad T, Khan A, Akhtar S. Ultrastructural study of peripheral and central stroma of keratoconus cornea. *Br J Ophthalmol*. 2017;101(6):845–850, doi:10.1136/bjophthalmol-2016-309834.
49. Daxer A, Fratzl P. Collagen fibril orientation in the human corneal stroma and its implication in keratoconus. *Invest Ophthalmol Vis Sci*. 1997;38(1):121–129.
50. White TL, Lewis PN, Young RD, et al. Elastic microfibril distribution in the cornea: differences between normal and keratoconic stroma. *Exp Eye Res*. 2017;159:40–48, doi:10.1016/j.exer.2017.03.002.
51. Pircher N, Schwarzhans F, Holzer S, et al. Distinguishing keratoconic eyes and healthy eyes using ultrahigh-resolution optical coherence tomography–based corneal epithelium thickness mapping. *Am J Ophthalmol*. 2018;189:47–54, doi:10.1016/j.ajo.2018.02.006.
52. Rocha KM, Perez-Straziota CE, Perez-Straziota E, Stulting RD, Randleman JB. SD-OCT analysis of regional epithelial thickness profiles in keratoconus, postoperative corneal ectasia, and normal eyes. *J Refract Surg Thorofare NJ 1995*. 2013;29(3):173–179, doi:10.3928/1081597X-20130129-08.
53. Reinstein DZ, Gobbe M, Archer TJ, Silverman RH, Coleman DJ. Epithelial, stromal, and total corneal thickness in keratoconus: three-dimensional display with artemis very-high frequency digital ultrasound. *J Refract Surg*. 2010;26(4):259–271, doi:10.3928/1081597X-20100218-01.
54. Yam GHF, Fuest M, Zhou L, et al. Differential epithelial and stromal protein profiles in cone and non-cone regions of keratoconus corneas. *Sci Rep*. 2019;9(1):2965, doi:10.1038/s41598-019-39182-6.
55. You J, Corley SM, Wen L, et al. RNA-Seq analysis and comparison of corneal epithelium in keratoconus and myopia patients. *Sci Rep*. 2018;8(1):389, doi:10.1038/s41598-017-18480-x.
56. Pahuja N, Kumar NR, Shroff R, et al. Differential molecular expression of extracellular matrix and inflammatory genes at the corneal cone apex drives focal weakening in keratoconus. *Invest Ophthalmol Vis Sci*. 2016;57(13):5372, doi:10.1167/iovs.16-19677.
57. D'Souza S, Nair AP, Sahu GR, et al. Keratoconus patients exhibit a distinct ocular surface immune cell and inflammatory profile. *Sci Rep*. 2021;11(1):20891, doi:10.1038/s41598-021-99805-9.
58. Jun AS, Cope L, Speck C, et al. Subnormal cytokine profile in the tear fluid of keratoconus patients. *PLoS One*. 2011;6(1):e16437, doi:10.1371/journal.pone.0016437.
59. Maycock NJR, Marshall J. Genomics of corneal wound healing: a review of the literature. *Acta Ophthalmol (Copenh)*. 2014;92(3):e170–e184, doi:10.1111/aos.12227.
60. Gross C, Le-Bel G, Desjardins P, Benhassine M, Germain L, Guérin SL. Contribution of the transcription factors Sp1/Sp3 and AP-1 to Clusterin gene expression during corneal wound healing of tissue-engineered human corneas. *Int J Mol Sci*. 2021;22(22):12426, doi:10.3390/ijms222212426.
61. Li Y, Ge L, Chen X, et al. The common YAP activation mediates corneal epithelial regeneration and repair

with different-sized wounds. *NPJ Regen Med*. 2021;6(1):16, doi:10.1038/s41536-021-00126-2.

62. Wilson SE, Medeiros CS, Santhiago MR. Pathophysiology of corneal scarring in persistent epithelial defects after PRK and other corneal injuries. *J Refract Surg Thorofare NJ 1995*. 2018;34(1):59–64, doi:10.3928/1081597X-20171128-01.
63. Chandrasekher G, Ma X, Lallier TE, Bazan HEP. Delay of corneal epithelial wound healing and induction of keratocyte apoptosis by platelet-activating factor. *Invest Ophthalmol Vis Sci*. 2002;43(5):1422–1428.
64. Desjardins P, Couture C, Germain L, Guérin SL. Contribution of the WNK1 kinase to corneal wound healing using the tissue-engineered human cornea as an in vitro model. *J Tissue Eng Regen Med*. 2019;13(9):1595–1608, doi:10.1002/term.2912.
65. Imamura R, Matsumoto K. Hepatocyte growth factor in physiology and infectious diseases. *Cytokine*. 2017;98:97–106, doi:10.1016/j.cyto.2016.12.025.
66. Miyagi H, Jalilian I, Murphy CJ, Thomasy SM. Modulation of human corneal stromal cell differentiation by hepatocyte growth factor and substratum compliance. *Exp Eye Res*. 2018;176:235–242, doi:10.1016/j.exer.2018.09.001.
67. Sumioka T, Iwanishi H, Okada Y, et al. Impairment of corneal epithelial wound healing is association with increased neutrophil infiltration and reactive oxygen species activation in tenascin X-deficient mice. *Lab Invest*. 2021;101(6):690–700, doi:10.1038/s41374-021-00576-8.
68. Puri S, Sun M, Mutoji KN, Gesteira TF, VJ Coulson-Thomas. Epithelial cell migration and proliferation patterns during initial wound closure in normal mice and an experimental model of limbal stem cell deficiency. *Invest Ophthalmol Vis Sci*. 2020;61(10):27, doi:10.1167/iovs.61.10.27.
69. Li CL, Yang D, Cao X, et al. Fibronectin induces epithelial-mesenchymal transition in human breast cancer MCF-7 cells via activation of calpain. *Oncol Lett*. 2017;13(5):3889–3895, doi:10.3892/ol.2017.5896.
70. Beeman N, Webb PG, Baumgartner HK. Occludin is required for apoptosis when claudin-claudin interactions are disrupted. *Cell Death Dis*. 2012;3:e273, doi:10.1038/cddis.2012.14.
71. Huttenlocher A, Lakonishok M, Kinder M, et al. Integrin and cadherin synergy regulates contact inhibition of migration and motile activity. *J Cell Biol*. 1998;141(2):515–526, doi:10.1083/jcb.141.2.515.
72. Foster JW, Shinde V, Soiberman US, et al. Integrated stress response and decreased ECM in cultured stromal cells from keratoconus corneas. *Invest Ophthalmol Vis Sci*. 2018;59(7):2977–2986, doi:10.1167/iovs.18-24367.
73. Kimura K, Kawano S, Mori T, et al. Quantitative analysis of the effects of extracellular matrix proteins on membrane dynamics associated with corneal epithelial cell motility. *Invest Ophthalmol Vis Sci*. 2010;51(9):4492–4499, doi:10.1167/iovs.09-4380.
74. Castro-Muñozledo F, Gómez-Flores E. Challenges to the study of asymmetric cell division in corneal and limbal epithelia. *Exp Eye Res*. 2011;92(1):4–9, doi:10.1016/j.exer.2010.11.002.
75. Mauser JF, Prehoda KE. Inscuteable regulates the pins-mud spindle orientation pathway. *PLoS One*. 2012;7(1):e29611, doi:10.1371/journal.pone.0029611.
76. Zhu ML, Kyprianou N. Role of androgens and the androgen receptor in epithelial-mesenchymal transition and invasion of prostate cancer cells. *FASEB J*. 2010;24(3):769–777, doi:10.1096/fj.09-136994.
77. Castoria G, D'Amato L, Ciociola A, et al. Androgen-induced cell migration: role of androgen receptor/filamin A association. *PloS One*. 2011;6(2):e17218, doi:10.1371/journal.pone.0017218.
78. Gorelick DA, Halpern ME. Visualization of estrogen receptor transcriptional activation in zebrafish. *Endocrinology*. 2011;152(7):2690–2703, doi:10.1210/en.2010-1257.
79. Ikeda K, Horie-Inoue K, Inoue S. Identification of estrogen-responsive genes based on the DNA binding properties of estrogen receptors using high-throughput sequencing technology. *Acta Pharmacol Sin*. 2015;36(1):24–31, doi:10.1038/aps.2014.123.
80. Suzuki T, Richards SM, Liu S, Jensen RV, Sullivan DA. Influence of sex on gene expression in human corneal epithelial cells. *Mol Vis*. 2009;15:2554–2569.
81. Chatzis N, Hafezi F. Progression of keratoconus and efficacy of pediatric [corrected] corneal collagen cross-linking in children and adolescents. *J Refract Surg Thorofare NJ 1995*. 2012;28(11):753–758, doi:10.3928/1081597X-20121011-01.
82. Gomes JAP, Tan D, Rapuano CJ, et al. Global consensus on keratoconus and ectatic diseases. *Cornea*. 2015;34(4):359–369, doi:10.1097/ICO.0000000000000408.
83. Soeters N, van der Valk R, Tahzib NG. Corneal cross-linking for treatment of progressive keratoconus in various age groups. *J Refract Surg Thorofare NJ 1995*. 2014;30(7):454–460, doi:10.3928/1081597X-20140527-03.
84. de Sanctis U, Loiacono C, Richiardi L, Turco D, Mutani B, Grignolo FM. Sensitivity and specificity of posterior corneal elevation measured by Pentacam in discriminating keratoconus/subclinical keratoconus. *Ophthalmology*. 2008;115(9):1534–1539, doi:10.1016/j.ophtha.2008.02.020.
85. Huang M, Kong X, Tang Z, et al. Cell cycle arrest induced by trichoplein depletion is independent of cilia assembly. *J Cell Physiol*. 2022;237(6):2703–2712, doi:10.1002/jcp.30693.
86. Waseem NH, Low S, Shah AZ, et al. Mutations in SPATA13/ASEF2 cause primary angle closure glaucoma. *PLoS Genet*. 2020;16(4):e1008721, doi:10.1371/journal.pgen.1008721.
87. Miller JE, Reese JC. Ccr4-Not complex: the control freak of eukaryotic cells. *Crit Rev Biochem Mol Biol*. 2012;47(4):315–333, doi:10.3109/10409238.2012.667214.
88. Priyadarsini S, McKay TB, Sarker-Nag A, Karamichos D. Keratoconus in vitro and the key players of the TGF-β pathway. *Mol Vis*. 2015;21:577–588.
89. Shi L, Stachon T, Käsmann-Kellner B, Seitz B, Szentmáry N, Latta L. Keratin 12 mRNA expression could serve as an early corneal marker for limbal explant cultures. *Cytotechnology*. 2020;72(2):239–245, doi:10.1007/s10616-020-00373-z.
90. Choi J, Kim H, Kim Y, et al. The anti-inflammatory effect of GV1001 mediated by the downregulation of ENO1-induced pro-inflammatory cytokine production. *Immune Netw*. 2015;15(6):291–303, doi:10.4110/in.2015.15.6.291.
91. Wu S, Majeed SR, Evans TM, et al. Clathrin light chains' role in selective endocytosis influences antibody isotype switching. *Proc Natl Acad Sci U S A*. 2016;113(35):9816–9821, doi:10.1073/pnas.1611189113.
92. Kobayashi T, Shiraishi A, Hara Y, et al. Stromal-epithelial interaction study: the effect of corneal epithelial cells on growth factor expression in stromal cells using organotypic culture model. *Exp Eye Res*. 2015;135:109–117, doi:10.1016/j.exer.2015.02.009.
93. Wong HL, Poon SHL, Bu Y, et al. A systematic review on cornea epithelial-stromal homeostasis. *Ophthalmic Res*. 2021;64(2):178–191, doi:10.1159/000509030.
94. Scarcelli G, Besner S, Pineda R, Kalout P, Yun SH. In vivo biomechanical mapping of normal and keratoconus corneas. *JAMA Ophthalmol*. 2015;133(4):480–482, doi:10.1001/jamaophthalmol.2014.5641.

Investigative Ophthalmology & Visual Science

95. Ziaei M, Gokul A, Vellara H, Lu LM, Patel DV, McGhee CNJ. Measurement of in vivo biomechanical changes attributable to epithelial removal in keratoconus using a noncontact tonometer. *Cornea*. 2020;39(8):946–951, doi:10.1097/ICO.0000000000002344.
96. Moshirfar M, Desautels JD, Walker BD, Murri MS, Birdsong OC, Hoopes PCS. Mechanisms of optical regression following corneal laser refractive surgery: epithelial and stromal responses. *Med Hypothesis Discov Innov Ophthalmol J*. 2018;7(1):1–9.
97. Stramer BM, Zieske JD, Jung JC, Austin JS, Fini ME. Molecular mechanisms controlling the fibrotic repair phenotype in cornea: implications for surgical outcomes. *Invest Ophthalmol Vis Sci*. 2003;44(10):4237–4246, doi:10.1167/iovs.02-1188.
98. Godefrooij DA, de Wit GA, Uiterwaal CS, Imhof SM, Wisse RPL. Age-specific incidence and prevalence of keratoconus: a nationwide registration study. *Am J Ophthalmol*. 2017;175:169–172, doi:10.1016/j.ajo.2016.12.015.
99. Mas Tur V, MacGregor C, Jayaswal R, O'Brart D, Maycock N. A review of keratoconus: diagnosis, pathophysiology, and genetics. *Surv Ophthalmol*. 2017;62(6):770–783, doi:10.1016/j.survophthal.2017.06.009.
100. Wagner H, Barr JT, Zadnik K. Collaborative Longitudinal Evaluation of Keratoconus (CLEK) study: methods and findings to date. *Contact Lens Anterior Eye J Br Contact Lens Assoc*. 2007;30(4):223–232, doi:10.1016/j.clae.2007.03.001.